



1 Hydrological and Runoff Formation Processes Based on Isotope
2 Tracing During Ablation Period in the Third Polar Region

3 Zong-Jie Li^{1*}, Zong-Xing Li^{2*}, Ling-Ling Song^{3*}, Jin-Zhu Ma^{1*}

4 ¹Key Laboratory of Western China's Environmental Systems (Ministry of Education), College of
5 Earth Environmental Science, Lanzhou University, Lanzhou, Gansu 730000, China

6 ²Key Laboratory of Ecohydrology of Inland River Basin/Gansu Qilian Mountains Ecology
7 Research Center, Northwest Institute of Eco-Environment and Resources, Chinese Academy of
8 Sciences, Lanzhou 730000, China

9 ³College of Forestry, Gansu Agricultural University, Lanzhou, Gansu 730070, China

10 *Corresponding author: Tel: 86+18993033525, E-mail: lzjie314@163.com (Zong-Jie Li),
11 lzxhhs@163.com (Zong-Xing Li).

12

13

14

15

16

17

18

19

20

21

22

23

24

25

26

27

28

29

30



31 **Abstract:** This study focused on the hydrological and runoff formation processes of
32 river water in the source regions of the Yangtze river during different ablation
33 episodes in 2016 and the ablation period from 2016 to 2018. The effects of altitude
34 were greater for the river in the glacier permafrost area than for the mainstream and
35 the permafrost area during the total ablation period in 2016. There was a significant
36 negative correlation (at the 0.01 level) between precipitation and $\delta^{18}\text{O}$, while a
37 significant positive correlation was evident between precipitation and d-excess. More
38 interestingly, significant negative correlations appeared between $\delta^{18}\text{O}$ and temperature,
39 relative humidity, and evaporation. A mixed segmentation model for end-members
40 was used to determine the proportion of the contributions of different water sources to
41 the target water body. The proportions of precipitation, supra-permafrost water, and
42 glacier and snow meltwater for the mainstream were 41.70%, 40.88%, and 17.42%,
43 respectively. The proportions of precipitation, supra-permafrost water, and glacier and
44 snow meltwater were 33.63%, 42.21%, and 24.16% for the river in the glacier
45 permafrost area and 20.79%, 69.54%, and 9.67%, respectively, for that in the
46 permafrost area. The supra-permafrost water was relatively stable during the different
47 ablation periods, becoming the main source of runoff in the alpine region, except for
48 precipitation, during the total ablation period.

49
50 **Keywords:** River water, stable isotope, ablation period, source region, Yangtze River

51

52 **1. Introduction**

53



54 Liquid precipitation, glaciers, snow, and permafrost in cold regions are important
55 components of hydrological processes, serve as a key link in the water cycle, and are
56 amplifiers and indicators of climate change (Yang et al., 2012; Chang et al., 2015; Li
57 et al., 2016a; 2016b; 2018). They are not only important as the recharge sources of
58 water in river basins but are also important resources to support regional development
59 (Halder et al., 2015; Lafrenière et al., 2019). The runoff system in the source area of
60 the Yangtze River consists of alpine glaciers, snow, frozen soil, and liquid
61 precipitation. The temporal and spatial variations of runoff components are of great
62 significance for water levels during wet and dry years in terms of ecological
63 protection and the distribution of water resources (Wang et al., 2012; Pan et al., 2017;
64 Mu et al., 2018). Therefore, studying changes in the composition of runoff and its
65 hydrological effect in cold areas can not only consolidate theories on runoff research,
66 prediction, and adaptation, but also have important practical significance for
67 construction, industry, and agriculture in cold regions (Wang et al., 2009; 2017; Wang
68 et al., 2019).

69

70 The stable isotope tracer technique has become an important research method in
71 hydrology. In recent years, the response of hydrological processes to climate change
72 in cold regions has become a hot topic in the field of global change, which has greatly
73 promoted the application of the stable isotope and chemical ion tracing methods in the
74 analysis of runoff in cold regions (Li et al., 2015; 2019; Qu et al., 2017; Zhu et al.,
75 2019). Liu et al. (2004) systematically studied the contribution of glacier and snow



76 meltwater to runoff in a cold area in Colorado, USA. It was found that the
77 contribution of glacier and snow meltwater to runoff in spring was as high as 82%.
78 Boucher and Carey (2010) systematically studied runoff segmentation in permafrost
79 basins. Maurya et al. (2011) found that the average contribution of meltwater to runoff
80 was 32% in typical glacial basins on the southern slope of the Himalayas. The
81 application of the stable isotope tracer method in the analysis of runoff components in
82 the cold regions of China has been relatively small. Gu and Longinelli (1993) first
83 used $\delta^{18}\text{O}$ as a tracer in the Urumqi River in the Tianshan Mountains. The recharge
84 water source can be separated into rainfall, snow meltwater, groundwater, and ice
85 melt water. The results showed that groundwater and snow melt water were the major
86 recharge sources of the Urumqi River in different periods and locations. Since then,
87 Kong and Pang (2012) have studied the contribution of meltwater to runoff and its
88 climatic sensitivity in two typical glacial basins in the Tianshan Mountains. The
89 composition of runoff from the Tizinafu River in the Tianshan Mountains shows that
90 the average contribution of snow melt water is 43% (Fan et al., 2015). The
91 contribution of glacier and snow meltwater to runoff in the Baishui River in the
92 Yulong Snow Mountains was 53.4% in summer (Pu et al., 2013). A study of the
93 Babao River and the Hulugou basin in the Qilian Mountains showed that different
94 water sources were fully mixed into groundwater before recharging rivers in this
95 alpine cold region, and that the contribution of meltwater in the cryosphere to runoff
96 in the cold region was as high as 33% (Li et al., 2014a; 2014b). Although these
97 studies determined the contribution of precipitation and glacier and snow meltwater to



98 runoff in the cold regions, they neglected the contribution of supra-permafrost water
99 to runoff and its impact on hydrological processes (Prasch et al., 2013; Lutz et al.,
100 2014). On the one hand, it increases the uncertainty of runoff analysis in the cold
101 regions. On the other hand, it is difficult to comprehensively evaluate the impact of
102 components on the runoff process and the hydrological effects in cold regions.

103

104 The source of the Yangtze River, which is a typical alpine frozen soil area, is an
105 important ecological barrier and a protected water source in China (Liang et al., 2008;
106 Li et al., 2017). The regional climate shows a significant warm and wet trend against
107 the background of global climate change. Regional evapotranspiration increases
108 because it is affected by this, and ice and snow resources exhibit an accelerating
109 melting trend (Kang et al., 2007; Wang et al., 2019). The ground temperature of the
110 permafrost increases, causing it to melt significantly. The active layer becomes thicker
111 and degenerates remarkably (Shi et al., 2019). Given this background, the temporal
112 and spatial patterns, mechanisms, and influences of precipitation, glacier and snow
113 meltwater, meltwater in the active layer, and groundwater in the region undergo
114 profound changes and impact runoff processes (Wu et al., 2015). These significant
115 impacts and their hydrological effects on the entire basin have gradually become
116 prominent.

117

118 In summary, due to the lack of data and the difficulty of observation and sampling in
119 cold regions, current studies have paid more attention to the study of hydrological



120 processes and water cycle characteristics at the watershed scale from the macroscopic
121 point of view. However, there is a lack of in-depth study on the mechanism of the
122 temporal and spatial variations of runoff components from the microscopic point of
123 view, and the understanding of its hydrological effects is still in the exploratory stage.
124 At present, although stable isotope tracer techniques have been applied to the analysis
125 of runoff in cold regions, most of the current studies are limited to the assessment of
126 the contribution and impact of glacier and snow melt water but neglect the significant
127 role of liquid precipitation increase and melt water in the active layer. The results in a
128 lack of systematic understanding of the hydrological effects of runoff composition
129 changes in cold regions. Meanwhile, different types of tributaries in runoff-producing
130 areas are the key to runoff-producing processes and are the main links to
131 understanding hydrological processes in cold regions. It is urgent to develop an
132 understanding of how runoff is produced. In addition, the current study of
133 hydrological processes in the source area of the Yangtze River focuses on the
134 variation in runoff itself and its response mechanism to climate change, lacking
135 in-depth analysis of runoff components and its hydrological effects. Therefore, taking
136 the source area of the Yangtze River as an example, we conduct a study into the
137 temporal and spatial variations of isotopes in different tributary rivers under the
138 background of climate warming and their influencing factors by using the methods of
139 field observation, experimental testing, stable isotope tracing, and analytical modeling
140 of end-element mixed runoff. Based on the conversion signals of stable isotopes in
141 each link of the runoff process, this study further explores the hydraulic relations,



142 recharge-drainage relations and their transformation paths, and the processes of each
143 water body, and determines the composition of runoff, quantifies the contribution of
144 each runoff component to different types of tributaries, and analyzes the hydrological
145 effects of the temporal and spatial variation of runoff components. On the one hand,
146 the research results can reveal the evolution mechanism of runoff in cold regions
147 under the background of climate warming. On the other hand, it provides parameter
148 support and a theoretical basis for the simulation and prediction of runoff changes in
149 cold regions, and then provides a scientific basis for a more systematic understanding
150 of the hydrological effects caused by underlying surface changes in cold regions,
151 ultimately providing decision-making basis for the rational development and
152 utilization of water resources in river basins.

153

154 **2. Data and Methods**

155

156 **2.1 Study area**

157

158 The source region of the Yangtze River is located in the hinterland of the Tibetan
159 Plateau (Fig. 1). It is an important ecological barrier and water conservation region in
160 China. The southern boundaries are the Tanggula Mountains and Sederi Peak, which
161 contain the watersheds of the Nujiang River and the Lancangjiang River, respectively.
162 The mean altitude reaches 4000 m above sea level with a decreasing elevation from
163 west to east (Yu et al., 2013) that covers an area of approximately 138,000 km²,
164 ~7.8% of the total area of the Yangtze River Basin. Most tributaries start from glaciers,
165 and form very dense drainage networks, such as those of the Chumaer River in the



166 north, Tuotuohe River in the middle, and Dangqu River in the south (Pu, 1994). The
167 glaciers in the study area are mainly distributed along the north-oriented slopes of the
168 Tanggula Mountains and Sedir Mountains and the south-oriented slopes of the
169 Kunlun Mountains, with a total area of 1496.04 km² (Yao et al., 2014). The
170 permafrost has a thickness of 10 – 120 m, which accounts for 77% of the total basin
171 area, and most surface soils are frozen during winter and thaw in summer, and active
172 layer thicknesses range from 1–4 m (Gao et al., 2012). Annual average temperatures
173 range from 3 – 5.5°C. The annual precipitation is 221.5 – 515 mm (Yu et al., 2014).
174 The mean annual precipitation varies considerably over the reserve, and ~80% of the
175 annual precipitation occurs during summer, with the highest precipitation occurring in
176 August.

177

178 **2.2 Sample Collection**

179

180 This study mainly collects precipitation, glacier and snow melt-water,
181 supra-permafrost water and river water to systematic analysis the recharge
182 relationship between precipitation, glacier and snow melt-water, supra-permafrost
183 water and river water in the source area of the Yangtze River. The specific sampling
184 process is as follows:

185

186 River water: In order to analysis the spatial and temporal characteristic of stable
187 isotope of river water in mainstream (25 samples) and major tributary (including river
188 in glacier permafrost area (105 samples) and river in permafrost area (167 samples))



189 in the study area, All of river water samples around the traffic routes in the source area
190 of the Yangtze River were collected in initial ablation in 2016 (48 samples), ablation
191 in 2016 (88 samples), end ablation in 2016 (45 samples), ablation in 2017 (55 samples)
192 and ablation in 2018 (61 samples) (Fig.1).

193

194 Glacier and snow melt-water: This paper researched the hydrochemistry characteristic
195 of melt-water in Cryosphere (Yuzhu peak Glacier, Geladandong Glacier and
196 Dongkemadi Glacier) through collected water samples by fixed-point sampling from
197 June to September in 2016 and 2017. The samples were collected once every 10 days
198 at the glacier front during the ablation period. The sampling time is at 14 o'clock per
199 day. The sampling location is in hydrological section at the end of the glacier.

200

201 Supra-permafrost water: Supra-permafrost water is the most widely distributed
202 groundwater type in the SRYR, and it is mainly stored in the permafrost active layer
203 (Li et al.,2018). The hydrochemistry characteristic of supra-permafrost water in the
204 study area this paper collected water samples by comprehensive sampling from June
205 to September in 2016 and 2018. The sampling process is manual operation. At first, a
206 2-m deep profile of the permafrost active layer was dug at each of the sampling points.
207 Then, the collection of the water samples are immediately filtered with 0.45 um
208 Millipore filtration membrane. Then, samples were poured the filtered into a clean
209 polyethylene bottle.

210



211 Precipitation: precipitation samples were collected at Zhimenda Hydrological Station
212 (ZMD) at the mountain pass of the source area of the Yangtze River, Qumalai
213 Meteorological Station(QML) in the middle reaches of the source area and Tuotuo
214 River Meteorological Station(TTH) in the upper reaches of the source area. The
215 sampling period extended from April 1, 2016 to October 31, 2018.

216

217 Before analysis, all samples were stored at 4°C in a refrigerator without evaporation.
218 Precipitation and surface water samples were analyzed for $\delta^{18}\text{O}$ and δD by means of
219 laser absorption spectroscopy (liquid water isotope analyzer, Los Gatos Research
220 DEL-100, USA) at the Key Laboratory of Ecohydrology of Inland River Basin,
221 Northwest Institute of Eco-Environment and Resources, CAS. The results are reported
222 relative to the Vienna Standard Mean Ocean Water (VSMOW). Measurement
223 precisions for $\delta^{18}\text{O}$ and δD were better than 0.5‰ and 0.2‰, respectively. Field
224 measurements included pH, dissolved oxygen (DO), electrical conductivity (EC), and
225 water temperature.

226

227 **2.3 EMMA**

228

229 Hooper (2003) introduced the end-member mixing analysis (EMMA) using
230 chemical/isotopic compositions in waters. The techniques involve graphical analyses,
231 in which chemical and isotopic parameters are used to represent the designated end
232 members. Tracer concentrations are constant in space and time. Essentially, the
233 composition of the water changing can be considered as a result of intersections



234 during its passage through each landscape zone. Tracers can be used to determine both
235 sources and flow paths. The EMMA tracer approach has been a common method for
236 analyzing potential water sources contributing to stream flow (Li et al, 2014a; 2016a).
237 Here in a three end-member mass-balance mixing model is employed to calculate the
238 contribution of up to three water sources in stream water, such as the following:

$$239 \quad X_S = F_1 X_1 + F_2 X_2 + F_3 X_3 \quad (1a)$$

$$240 \quad Y_S = F_1 Y_1 + F_2 Y_2 + F_3 Y_3 \quad (1b)$$

241 In Eq. (1), X and Y represent concentrations of two types of different tracers. In this
242 study, $\delta^{18}\text{O}$ and deuterium excess were chosen for comparison. The subscripts
243 represents stream water sample, and 1, 2, and 3 represent water from the respective
244 contribution of three respective source waters (end members) to stream water. The
245 fraction of each end-member is denoted by F. The solutions for F_1 , F_2 , and F_3 in
246 regards to tracer concentrations in Eq. (1) can be given as:

$$247 \quad F_1 = [(X_3 - X_S)/(X_3 - X_2) - (Y_3 - Y_S)/(Y_3 - Y_2)] / [(Y_1 - Y_3)/(Y_3 - Y_2) - (X_1 - X_3)/(X_3 - X_2)] \quad (2a)$$

$$248 \quad F_2 = [(X_3 - X_S)/(X_3 - X_1) - (Y_3 - Y_S)/(Y_3 - Y_1)] / [(Y_2 - Y_3)/(Y_3 - Y_1) - (X_2 - X_3)/(X_3 - X_1)] \quad (2b)$$

$$249 \quad F_3 = 1 - F_1 - F_2 \quad (2c)$$

250 This method has been used by previous study (Li et al., 2014b; 2015; 2016b). This
251 study also used this method to evaluate the contribution of possible sources to the
252 river water.

253

254 **2.4 Uncertainty in hydrograph separation**

255

256 The uncertainty of tracer-based hydrograph separations can be calculated using the
257 error propagation technique (Genereux, 1998; Klaus & McDonnell, 2013). This
258 approach considers errors of all separation equation variables. Assuming that the



259 contribution of a specific streamflow component to streamflow is a function of several
260 variables c_1, c_2, \dots, c_n and the uncertainty in each variable is independent of the
261 uncertainty in the others, the uncertainty in the target variable (e.g., the contribution of
262 a specific streamflow component) is estimated using the following equation (Genereux,
263 1998; Uhlenbrook & Hoeg, 2003):

$$264 \quad W_{f_x} = \sqrt{\left(\frac{\partial z}{\partial c_1} W_{c_1}\right)^2 + \left(\frac{\partial z}{\partial c_2} W_{c_2}\right)^2 + \dots + \left(\frac{\partial z}{\partial c_n} W_{c_n}\right)^2}, \quad (3)$$

265 where W represents the uncertainty in the variable specified in the subscript. f_x is the
266 contribution of a specific streamflow component x to streamflow. The software
267 package MATLAB is used to apply equation 3 to the different hydrograph separations
268 in this study.

269

270 **3. Results**

271

272 **3.1 Temporal Variation**

273

274 As shown in Fig. 2, there was significant difference in $\delta^{18}\text{O}$ and d-excess in the
275 different ablation events in 2016 and total ablation from 2016 to 2018 for the different
276 types of runoff. For the mainstream, the order of $\delta^{18}\text{O}$ for the different ablation
277 periods was initial ablation (-10.31‰) > final ablation (-12.22‰) > total ablation
278 (-13.51‰), while the order of $\delta^{18}\text{O}$ in ablation from 2016 to 2018 was total ablation
279 in 2018 (-11.21‰) > total ablation in 2017 (-13.20‰) > total ablation in 2016
280 (-13.51‰). The order of d-excess for the different ablation periods and total ablation



281 from 2016 to 2018 was: total ablation (13.57‰) > initial ablation (12.71‰) > final
282 ablation (12.35‰) and total ablation in 2017 (14.62‰) > total ablation in 2016
283 (13.57‰) > total ablation in 2018 (10.81‰) (Fig. 2a, d). For the river in the glacier
284 permafrost area, the order of $\delta^{18}\text{O}$ for the different ablation periods and the total
285 ablation from 2016 to 2018 was the same as the mainstream order, but the values of
286 $\delta^{18}\text{O}$ were different for the mainstream. The $\delta^{18}\text{O}$ values for the initial ablation in
287 2016, total ablation in 2016, final ablation in 2016, total ablation in 2017, and total
288 ablation in 2018 were -9.92‰ , -13.29‰ , -10.82‰ , -12.38‰ , and -11.04‰ ,
289 respectively. The order of d-excess for the different ablation periods and total ablation
290 from 2016 to 2018 was: total ablation (14.24‰) > initial ablation (13.02‰) > final
291 ablation (10.58‰) and total ablation in 2016 (14.24‰) > total ablation in 2017
292 (12.40‰) > total ablation in 2018 (10.49‰) (Fig. 2b, e). For the river in the
293 permafrost area, the order of $\delta^{18}\text{O}$ for the different ablation periods and ablation from
294 2016 to 2018 was: initial ablation (-10.02‰) > final ablation (-11.65‰) > total
295 Ablation (-12.53‰) and total ablation in 2018 (-11.17‰) > total ablation in 2017
296 (-11.99‰) > total ablation in 2016 (-12.53‰). This was the same as for the
297 mainstream and the river in the glacier permafrost area. However, the order of
298 d-excess for the river in the permafrost area was different than that for the river in the
299 glacier permafrost area. This order, for the different ablation periods and ablation
300 from 2016 to 2018, was as follows: final ablation (13.61‰) > total ablation
301 (12.25‰) > initial ablation (9.97‰), and total ablation in 2017 (13.57‰) > total
302 ablation in 2016 (12.25‰) > total ablation in 2018 (9.72‰) (Fig. 2c, f). In general,



303 the $\delta^{18}\text{O}$ in the mainstream was more negative than those in the rivers in the glacier
304 permafrost and permafrost areas. These results may be due to the fact that the highest
305 runoff was for the mainstream and that the effects of dilution result in lower isotope
306 values. However, the $\delta^{18}\text{O}$ in the river in the glacier permafrost area was more
307 positive than those in the mainstream and the river in the permafrost area. The effect
308 of evaporation could explain these results and the change in d-excess could also
309 demonstrate the same.

310

311 **3.2 Spatial Variation**

312

313 To analyze the spatial variation of $\delta^{18}\text{O}$ based on the different ablation periods in 2016
314 and total ablation from 2016 to 2018, spatial interpolation of all river water samples in
315 the study area was performed using ArcGIS. The results are shown in Fig. 3. The $\delta^{18}\text{O}$
316 value in the north-central region of the study area was more positive than those in
317 other regions. In the southeastern part of the study area, especially the QML, ZMD,
318 and Tanggula Mountains, the values were more negative during the initial ablation
319 period. The area of positive ablation during the total ablation period, which was
320 concentrated mainly in the northeast part of the study area, was larger than that during
321 the initial ablation. The other regions, except some areas in the southwest, turned
322 positive. The area of positive ablation was largest during the final of the different
323 ablation periods in 2016; all areas, except some in the eastern region of the study area,
324 were positive (Fig. 3). The area of positive ablation in the central and northern regions
325 began to expand in 2017 compared to the area of total ablation in 2016. Furthermore,



326 the area of negative ablation appears mainly in the southeastern and southwestern
327 portions of the study area. However, the positive ablation area was also concentrated
328 in the central and northern regions in 2018 and it was greater than it was in 2016 and
329 2017. Meanwhile, the negative ablation area appeared mainly in the southeastern and
330 southwestern portions of the study area, but it was smaller than in 2016 and 2017.
331 These results may be related to evaporation, possible recharge sources, or
332 meteorological factors. These results were comprehensive and influenced by
333 meteorological factors and the type and proportion of recharge sources. The
334 evaporation effect was strong in the central and northern regions, which were also the
335 major glacier and permafrost regions. The southeastern region was the downstream
336 area where all runoff converged; thus, the dilution effect led to a more negative $\delta^{18}\text{O}$
337 here. Moreover, the Tanggula Mountains, with altitudes higher than those in other
338 regions, were located southwest of the study area; thus, evaporation had a low
339 influence on this region and the oxygen stable isotopes were more negative.

340

341 Just as with the spatial distribution of $\delta^{18}\text{O}$, there was a significant spatial distribution
342 of d-excess in the study area (Fig. 4). Compared to the spatial distribution of $\delta^{18}\text{O}$, the
343 d-excess in the central and northern regions were lower than those in the other regions.
344 However, d-excess was higher in the latter, especially in the southwestern regions and
345 in the southeastern regions during the initial ablation period. The lower area begin to
346 expand during the total ablation period in 2016, while the central and northeastern
347 regions and the Tanggula Mountains were greater. Meanwhile, the negative ablation



348 area continued to expand during the final ablation period; ablation was greater only in
349 the southeastern part of the study area. However, all regions exhibited high ablation,
350 especially in the Tanggula Mountains, except for areas in the eastern region where the
351 ablation was low during the ablation period in 2017. Moreover, the lower ablation
352 regions appeared mainly in the central and southeastern regions of the study area;
353 values were higher in the other regions, especially in the Tanggula Mountains and the
354 northeast. The spatial distribution of d-excess also confirmed the spatial distribution
355 of the oxygen stable isotope because evaporation resulted in the enrichment of
356 isotopes and led to a reduction in d-excess.

357

358 In general, the influence of evaporation on the isotope and d-excess was only
359 manifested in some places, such as the central and northern parts of the study area, in
360 the initial ablation and the total ablation periods. However, the influence of
361 evaporation on the isotope and d-excess was manifested in most places, except the
362 southeast of the study area. Meanwhile, these results also indicated that there may be
363 a hysteresis for the influence of meteorological factors on isotopes and d-excess. On
364 the one hand, river water was the result of the final convergence of various recharge
365 sources that include precipitation, supra-permafrost water, and glacier and snow
366 meltwater. On the other hand, meteorological factors directly affected the main
367 recharge sources of river water.

368

369 As shown in Fig. 6, there was a significant difference in the variation of $\delta^{18}\text{O}$ and



370 d-excess with altitude for the mainstream, the river in the glacier permafrost area, and
371 the river in the permafrost area of the study area. For the mainstream, the oxygen
372 stable isotope showed a decreasing trend, with increases in altitude, during the
373 ablation periods in 2016 and 2018. In other words, the altitude effect only appeared in
374 the total ablation periods during these two years and had values of $-0.16\text{‰}/100\text{ m}$
375 ($p < 0.05$) and $-0.14\text{‰}/100\text{ m}$ ($p < 0.05$), respectively. However, $\delta^{18}\text{O}$ showed an
376 increasing trend with an increase in altitude during the initial and final ablation
377 periods in 2016 and total ablation period in 2017. The anti-altitude effects of the
378 initial and final ablation periods in 2016, and total ablation period in 2017, were
379 $0.11\text{‰}/100\text{ m}$ ($p < 0.05$), $0.13\text{‰}/100\text{ m}$ ($p < 0.01$), and $0.04\text{‰}/100\text{ m}$ ($p < 0.05$),
380 respectively. d-excess showed a decreasing trend during the initial and final ablation
381 periods in 2016 and a significant increasing trend in the total ablation period from
382 2016 to 2018. For the river in the glacier permafrost area, $\delta^{18}\text{O}$ showed a decreasing
383 trend with increase in altitude during the total ablation periods in 2016 and 2018, but
384 the ablation in 2018 was not significant. The altitude effect was $-0.66\text{‰}/100\text{ m}$
385 ($p < 0.05$) and $-0.15\text{‰}/100\text{ m}$ ($p > 0.05$), respectively, during the former two periods.
386 Moreover, a significant anti-altitude effect of $0.47\text{‰}/100\text{ m}$ ($p < 0.05$), $0.67\text{‰}/100\text{ m}$
387 ($p < 0.05$), and $0.97\text{‰}/100\text{ m}$ ($p < 0.05$), appeared in the initial and final ablation
388 periods in 2016 and total ablation period in 2017, respectively. Just as with the
389 mainstream, d-excess showed a decreasing trend in the initial and final ablation
390 periods in 2016 and an increasing trend in the total ablation from 2016 to 2018. For
391 the river in the permafrost area, $\delta^{18}\text{O}$ showed a decreasing trend with an increase in



392 altitude in the initial ablation period and total ablation period in 2016, with an altitude
393 effect of $-0.38\text{‰}/100\text{ m}$ ($p < 0.05$) and $-0.12\text{‰}/100\text{ m}$ ($p > 0.05$), respectively.
394 However, $\delta^{18}\text{O}$ showed an increasing trend with increase in altitude in the final
395 ablation period in 2016 and the total ablation periods in 2017 and 2018, with an
396 anti-altitude effect of $0.21\text{‰}/100\text{ m}$ ($p < 0.05$), $0.01\text{‰}/100\text{ m}$ ($p > 0.05$), and
397 $0.68\text{‰}/100\text{ m}$ ($p < 0.05$), respectively. d-excess showed an increasing trend with
398 increase in altitude in the initial and final ablation periods in 2016 and total ablation
399 periods in 2016 and 2017. However, d-excess also showed a decreasing trend with
400 increase in altitude in the total ablation period in 2018.

401

402 In summary, the altitude effect mainly appeared during ablation, whether it was in the
403 mainstream, the river in the glacier permafrost area, or the river in the permafrost area.
404 The altitude effects were higher for the river in the glacier permafrost area than for the
405 mainstream or the river in the permafrost area during the ablation period in 2016.
406 Meanwhile, the anti-altitude effect of the river in the glacier permafrost area was
407 higher than that of the other areas. The $\delta^{18}\text{O}$ during the initial and final ablation
408 periods in 2016 showed a significant anti-altitude effect for the mainstream and the
409 river in the glacier permafrost area; a significant altitude effect appeared during the
410 initial ablation period for the river in the permafrost area. These results may be due to
411 the comprehensive influence of possible recharge sources and different recharge
412 proportions caused by the influence of meteorological factors.

413



414 **3.3 Evaporation Line**

415

416 The variations in the location of the evaporation line for river water during the
417 different ablation periods in 2016 and the total ablation periods from 2016 to 2018 are
418 shown in Fig. 6. The slope and intercept of the LEL for river water showed an
419 increasing trend from the initial to final ablation periods in 2016. The LEL in the
420 initial ablation period was $\delta D = 6.59\delta^{18}O - 3.60$ ($p < 0.01$) and it was
421 $\delta D = 6.88\delta^{18}O - 1.37$ ($p < 0.01$) during the total ablation period. The LEL during the
422 final ablation period was $\delta D = 7.39\delta^{18}O + 5.88$ ($p < 0.01$). These results indicate that
423 the effect of evaporation on the stable isotopes in river water gradually weakened
424 from the initial ablation to the final ablation periods. The slope and intercept of the
425 LEL of river water during the total ablation period in 2017 were lower than those in
426 2016. The LEL during the total ablation period in 2017 was $\delta D = 6.59\delta^{18}O - 3.63$
427 ($p < 0.01$). However, whether the slope or the intercept of LEL of river water in 2018
428 was higher than that in 2016 and 2017, with the LEL was: $\delta D = 7.63\delta^{18}O + 5.82$
429 ($p < 0.01$). This phenomenon showed that the influence of evaporation on stable
430 isotope levels was greatest during the total ablation period in 2017, followed by that
431 in 2016. In general, the lower slope and intercept indicate that the water body was
432 affected by evaporation or non-equilibrium dynamic fractionation. This conclusion
433 could also explain the results of this study.

434

435 **3.4 Recharge Sources**

436



437 The distributions of δD and $\delta^{18}O$ for river water in the different types of water, among
438 supra-permafrost water, glacier snow meltwater, and precipitation, are shown in Fig. 8
439 the different ablation periods in 2016 and ablation from 2016 to 2018. The results of
440 the distribution of δD and $\delta^{18}O$ of river water indicate the possible recharge sources of
441 river water. However, the δD and $\delta^{18}O$ of river water, supra-permafrost water, glacier
442 snow meltwater, and precipitation exhibited little change during the initial ablation in
443 2016 (Fig. 7a, b). This phenomenon suggests that precipitation may be the major
444 recharge sources for river water during the initial ablation. A plot of δD versus $\delta^{18}O$
445 for river and supra-permafrost water, glacier snow meltwater, and precipitation is
446 shown in Fig. 8c. The δD and $\delta^{18}O$ values of glacier and snow meltwater from above
447 the LMWL are the most negative compared to other water bodies. The stable isotope
448 of supra-permafrost water was relatively more positive, located below the LMWL,
449 confirming the influence of strong evaporation. The stable isotope of river water was
450 close to the LMWL, and its concentration value was between precipitation, glacier
451 and snow meltwater, and supra-permafrost water, reflecting that river water was
452 recharged and affected by multi-source water in the study area. Moreover, the
453 distribution of river water, glacier and snow meltwater, and supra-permafrost water
454 also indicated that there was a hydraulic relationship between the source and target in
455 the different ablation periods in 2016 and ablation from 2016 to 2018.

456

457 The mixed segmentation model of the end-member is used to determine the
458 contribution proportions of different water sources to the target water. Owing to the



459 two stable isotope concentrations in different water bodies have significant spatial and
460 temporal differences, which can effectively distinguish different water bodies and
461 their mixing relationships. The d-excess and $\delta^{18}\text{O}$ are used as tracers of the mixed
462 segmentation model of the end-elements. As shown in Fig. 8, according to the
463 locations of the different types of water (mainstream, glacier permafrost area river,
464 and permafrost area river) and the distance from other water bodies (precipitation,
465 glacier and snow meltwater, and supra-permafrost water), which reflected the mixed
466 recharge of three water bodies, supra-permafrost water was the first end element,
467 precipitation was the second end element, and glacier and snow meltwater was the
468 third end element in the initial ablation in 2016. However, the possible recharge
469 sources of the mainstream, the glacier permafrost area river, and the permafrost area
470 river were different (Fig. 8), as the different runoffs likely have different recharge
471 sources and different recharge proportions. Overall, the source of the permafrost area
472 river was mainly the supra-permafrost water, with similar levels of precipitation in the
473 different periods of ablation in 2016 and the total ablation from 2016 to 2018. The
474 permafrost area river had the least contribution from the glacier and snow meltwater,
475 indicating that the supra-permafrost water was the major recharge source for the
476 permafrost area river followed by precipitation, and the recharge proportions also
477 exhibited the same trend. As the source of the glacier permafrost area river was the
478 same as the permafrost area river, the permafrost area river was dominated by the
479 supra-permafrost water, followed by precipitation and then glacier and snow
480 meltwater. However, the glacier permafrost area river comprised glacier and snow



481 meltwater more so in the total ablation period than in other periods. Compared with
482 the permafrost area river and the glacier permafrost area river, the mainstream was
483 governed by the supra-permafrost water in the initial ablation period while containing
484 nearly equal proportions of supra-permafrost water and precipitation in the final
485 ablation period. However, the mainstream received significant contributions from all
486 three end members in the total ablation period from 2016 to 2018 and particularly in
487 2017.

488

489 The recharge proportions of precipitation, supra-permafrost water, and glacier and
490 snow meltwater at different altitudes are depicted in Fig. 9, from the mixed
491 segmentation model of the three end-members during the ablation periods mentioned
492 above. The recharge proportions of the three end members in the ablation periods
493 were significantly different. This may be due to the different effects of the runoff
494 recharge sources in different ablation periods, as well as the significant differences in
495 recharge and drainage relationships in the different ablation periods. The recharge
496 proportions of precipitation in the initial ablation in 2016, total ablation in 2016, final
497 ablation in 2016, total ablation in 2017, and total ablation in 2018, obtained by
498 calculating the average contribution proportion from each altitude, were 28.71%,
499 44.41%, 44.60%, 42.53%, and 51.03%, respectively. Meanwhile, the recharge
500 proportions of supra-permafrost water in the initial ablation in 2016, total ablation in
501 2016, final ablation in 2016, total ablation in 2017, and total ablation in 2018 were
502 55.38%, 36.51%, 40.21%, 37.56%, and 28.87%, respectively. The recharge



503 proportions of glacier and snow meltwater in the initial ablation in 2016, total ablation
504 in 2016, final ablation in 2016, total ablation in 2017, and total ablation in 2018 were
505 15.91%, 19.08%, 15.19%, 19.90%, and 20.09%, respectively. The recharge proportion
506 of precipitation decreased with increase in altitude in the initial ablation, while the
507 proportion of supra-permafrost water and glacier and snow meltwater exhibited an
508 increasing trend with increase in altitude. However, the recharge proportion of the
509 supra-permafrost water was higher than that of precipitation or glacier and snow
510 meltwater, and also showed a decreasing trend from low to high altitude in the final
511 ablation in 2016. The proportion of glacier and snow meltwater increased with
512 increase in altitude, but the recharge proportion of supra-permafrost water was stable
513 with the change in altitude in the final ablation in 2016. The trend of precipitation and
514 glacier and snow meltwater for the total ablation was the same as that for the initial
515 and final ablation. However, the recharge proportion of precipitation was higher than
516 the proportion of supra-permafrost water and glacier and snow meltwater in the
517 ablation period. Meanwhile, the recharge proportion of glacier and snow meltwater in
518 ablation was higher than that in the initial and final ablation period. In general, the
519 recharge of supra-permafrost water to runoff was stable, whether in the different
520 ablation periods in 2016 or the total ablation from 2016 to 2018. However, the
521 proportion of supra-permafrost water was relatively low, mainly due to the larger
522 runoff during the ablation period.

523

524 Using the approach shown in Equation (3), the uncertainty originating from the
525 variation in the tracers of components and measurement methods could be calculated



526 separately (Uhlenbrook & Hoeg, 2003; Pu et al., 2013). According to the calculations
527 made using Equation (3), the uncertainty was estimated to be 0.07 for the three -
528 component mixing model in the study region. The uncertainty terms for
529 supra-permafrost water accounted for more than 50.0% of the total uncertainty,
530 indicating that the $\delta^{18}\text{O}$ and δD variations of supra-permafrost water accounted for the
531 majority of the uncertainty. Although there is some uncertainty for hydrograph
532 separation, isotope-based hydrograph separations are still valuable tools for evaluating
533 the contribution of meltwater to water resources, and they are particularly helpful for
534 improving our understanding of hydrological processes in cold regions, where there is
535 a lack of observational data.

536

537 **4. Discussions**

538

539 **4.1 Meteorological Factors**

540

541 To further explain the reason for the variation in temporal and spatial characteristics
542 of stable isotopes and LEL, this study includes the analysis of the monthly change in
543 precipitation, temperature, relative humidity, and evaporation during the sampling
544 period (from January 2016 to December 2018). The results are shown in Fig. 10. The
545 average of the precipitation was 371.9 mm during the sampling period, and the
546 precipitation in the total ablation period accounted for 78.87%. The average of the
547 temperature, relative humidity, and evaporation during the sampling period were
548 -1.42 °C, 52.20%, and 4.14 mm, respectively. However, the average of the
549 temperature, relative humidity, and evaporation during the total ablation period were



550 8.04 °C, 66.47%, and 5.57 mm, respectively.

551

552 More importantly, the precipitation during the initial, total, and final ablation periods
553 in 2016, and the total ablation periods in 2017 and 2018, were 50.40 mm, 107.90 mm,
554 42.90 mm, 70.60 mm, and 119.00 mm, respectively. For precipitation, the isotope
555 levels tend to decrease with the increase in rainfall; Precipitation is also the major
556 source of water for all water bodies (Maurya et al., 2011; Pu et al., 2013; Li et al.,
557 2014b; 2015; 2016a; 2018; Pan et al., 2017) and, in general, more precipitation
558 resulted in a greater dilution effect. A more negative $\delta^{18}\text{O}$ appeared in the total
559 ablation period in 2016 whether in all three study areas given the change in $\delta^{18}\text{O}$ (Fig.
560 2). This result showed that dilution does not only play an important role in the
561 precipitation effect; it also affects river water. However, the dilution effect was also
562 significant when precipitation was the major recharge source for river water
563 (Abongwa and Atekwana, 2018; Li et al., 2015).

564

565 Temperature for the initial, total, and final ablation periods in 2016, and the total
566 ablation periods in 2017 and 2018, were 6.82 °C, 9.58 °C, 3.77 °C, 9.47 °C, and
567 11.09 °C, respectively. For atmospheric precipitation, the lower the temperature was,
568 the higher the condensation degree of water vapor exhibited and the lower the isotope
569 content in precipitation. Therefore, there is a positive correlation between the stable
570 isotope and temperature in precipitation (Li et al., 2016a). However, the influence of
571 temperature on the stable isotope of river water was not significant from the variation



572 in river water isotope during the different ablation periods. However, the variation
573 trend of the stable isotope of river water in the total ablation period from 2016 to 2018
574 was similar to that for the change in temperature. Meanwhile, the variation trend of
575 d-excess can also be confirmed by this analysis (Fig. 2).

576

577 Relative humidity in the initial ablation, total ablation, and final ablation periods in
578 2016 and the total ablation periods in 2017 and 2018 were 60.07%, 63.16%, 70.57%,
579 63.39%, and 63.48%, respectively. When the relative humidity is low, the dynamic
580 fractionation increases and the slope decreases, and vice versa. The variation trend of
581 the slope of the LEL for the different ablation periods in 2016 was the same as that for
582 the change in relative humidity (Fig. 6). Meanwhile, the intercept of the LEL for the
583 different ablation periods in 2016 also showed the same trend.

584

585 Evaporation in the initial ablation, total ablation, and final ablation periods in 2016
586 and total ablation periods in 2017 and 2018 were 6.69 mm, 6.96 mm, 4.02 mm,
587 6.48 mm, and 6.02 mm, respectively. The stable isotopes of hydrogen and oxygen in
588 river water are comprehensively affected by the evaporation process, runoff change,
589 precipitation recharge, glacier and snow meltwater recharge, supra-permafrost water,
590 and evaporation loss in cold regions. During the process of evaporation, lighter water
591 isotopes are separated preferentially from the surface of water while heavier isotopes
592 are enriched in the remaining water body. Evaporation enriches the oxygen and
593 hydrogen stable isotopes and reduces excess deuterium (Li et al., 2015; 2018). The



594 trend in the oxygen isotope in the total ablation periods from 2016 to 2018 was the
595 same as that for the change in evaporation (Fig. 2). Meanwhile, the spatial distribution
596 of $\delta^{18}\text{O}$ and d-excess also responded to this change (Fig. 3, 4).

597

598 To further analyze the influence of meteorological factors on the stable isotope, the
599 correlation analysis between meteorological factors and the monthly value of $\delta^{18}\text{O}$
600 and d-excess, which showed continuous observations at two fixed-point stations was
601 analyzed (Table 1), and the results are shown in Table 1. There was a significant
602 negative correlation between precipitation and $\delta^{18}\text{O}$ at the 0.01 level (2-tailed), while
603 a significant positive correlation between precipitation and d-excess was also present.
604 More interestingly, just as with precipitation, a significant negative correlation
605 appeared between $\delta^{18}\text{O}$ and temperature, relative humidity, and evaporation, with
606 coefficients of -0.671 , -0.555 , and -0.636 , respectively. Meanwhile, a significant
607 positive correlation occurred between d-excess and temperature, relative humidity,
608 and evaporation, with coefficients of 0.602 , 0.524 , and 0.533 , respectively. This
609 results indicated that the direct influence of meteorological factors on stable isotopes
610 of river water was significant and definite.

611

612 Hydrogen and oxygen isotope compositions in river water are the result of the
613 combined effects of the isotopes making up present in precipitation, glacier and snow
614 meltwater, and supra-permafrost water as well as evaporative fractionation (Li et al.,
615 2015). The main influential hydrometeorological factors include precipitation,



616 temperature, relative humidity, and evaporation. On the whole, river water isotopes
617 were not influenced by a single factor; instead, they were based on the comprehensive
618 influence of many factors in the cold regions. The influence of meteorological factors
619 on different types of river water (mainstream, rivers in glacier permafrost areas, and
620 rivers in permafrost areas) showed that apart from their directly influences, each
621 factor indirectly affected the river water recharge source. This indirect influence was
622 mainly felt on precipitation, glacier, snow, and permafrost.

623

624

625 **4.2 Hydrological processes**

626

627 To systematically quantify the main recharge sources of different types of runoff in
628 the alpine regions, the possible sources and recharge proportions of runoff of different
629 types in different ablation periods were deeply analyzed by using the mixed
630 segmentation model of the three end-members in this study. The conceptual model
631 map of the recharge form and proportion of the river water in the different ablation
632 periods is shown in Fig. 11.

633

634 For the river in the glacier permafrost area, there was a significant difference in the
635 recharge proportion in the runoff area, in which there were several glaciers and
636 permafrost in the basin, and other areas during the various ablation periods. The
637 proportion of recharge from precipitation during the initial, total, and final ablations in
638 2016, the total ablation in 2017, and the total ablation in 2018 were 27.69%, 33.71%,



639 32.38%, 33.21%, and 41.48%, respectively. However, the proportion of
640 supra-permafrost water in the initial, total, and final ablations in 2016, the total
641 ablation in 2017, and the total ablation in 2018 were 54.68%, 35.96%, 32.38%,
642 33.21%, and 41.48%, respectively. The proportions of glacier and snow meltwater in
643 the initial, total, and final ablations in 2016, the total ablation in 2017, and the total
644 ablation in 2018 were 17.63%, 30.33%, 21.24%, 29.39%, and 22.19%, respectively.
645 These results show that supra-permafrost water was the important recharge source for
646 runoff during the initial and final ablation periods. The proportion of supra-permafrost
647 water was 50.53% during the initial and final ablation periods. It was also the next
648 highest source of runoff recharge, next to precipitation, during the ablation from 2016
649 to 2018; the proportions were 36.13% and 36.66%, respectively. The recharge
650 proportions for glacier and snow meltwater was higher during the total ablation period
651 than in the initial and final ablation periods, at 19.44% and 27.30%, respectively.
652
653 For permafrost area river, the runoff area only with permafrost and no glacier in the
654 basin, there was also an obvious difference for the recharge proportion in different
655 ablation period. Compared with the glacier permafrost area river the recharge
656 proportion of supra-permafrost water was higher for permafrost area river than that
657 for the glacier permafrost area river (42.21%). The recharge proportion of
658 supra-permafrost water was 69.54%. With the same as the glacier permafrost area
659 river, the supra-permafrost water was the important recharge sources to runoff in the
660 initial and final ablation, and the proportion was 80.97% in the initial and final



661 ablation period. Meanwhile, the proportion of supra-permafrost water was 61.92% in
662 the total ablation period. The proportion was higher than that for precipitation
663 (24.13%) in the total ablation period. In general, the supra-permafrost water was the
664 major recharge source for the permafrost area river in the different ablation periods in
665 the study area. Meanwhile, the glacier and snow meltwater had little contribution to
666 the permafrost area river in the initial and final ablation periods.

667

668 For the mainstream, the recharge proportions for precipitation during the initial, total,
669 and final ablations in 2016, the total ablation in 2017, and the total ablation in 2018
670 were 28.67%, 48.35%, 43.18%, 46.97%, and 41.33%, respectively. The proportion
671 was 35.93% in the initial and final ablation periods and 45.55% in the total ablation
672 period. However, the proportions of supra-permafrost water during the initial, total,
673 and final ablation in 2016, the total ablation in 2017, and the total ablation in 2018
674 were 52.37%, 33.52%, 42.61%, 39.68%, and 38.21%, respectively. The proportion
675 was 47.49% during the initial and final ablation periods and 36.47% during the total
676 ablation period. These results indicate that, for the study area, the supra-permafrost
677 water was the major recharge source for the mainstream in the first two of these
678 ablation periods while precipitation was the major recharge source for the mainstream
679 in the total ablation period. The proportions of glacier and snow meltwater during the
680 initial, total, and final ablation in 2016, the total ablation in 2017, and the total
681 ablation in 2018 were 18.96%, 20.13%, 14.21%, 13.35%, and 20.46%, respectively.
682 The proportion of glacier and snow meltwater for the mainstream (16.59%) was



683 higher than that for the river in the permafrost area (3.25%) but lower than that for the
684 river in the glacier permafrost area (19.44%) during the initial and final ablation
685 periods. The former proportion was also higher than that for the river in the
686 permafrost area (17.98% vs 13.95%) but lower than that for the river in the glacier
687 permafrost area (27.30%) during the total ablation period.

688

689 The hydrological process in cold regions has one particularity. The low permeability
690 in permafrost layer and the freeze-thaw depths of the soil reduces soil infiltration (Wu
691 et al., 2015; Wang et al., 2019). Therefore, the rapid replenishment of meltwater by
692 runoff results in a difference in the runoff generation mechanism in the permafrost
693 and non-permafrost regions (Yang et al., 2010; Li et al., 2018). Moreover, because the
694 freeze-thaw depths of the soil changes with annual fluctuations in temperature, there
695 is an effect on soil water storage capacity that results in a difference in the runoff
696 generation mechanism during different ablation periods (Wang et al., 2019). Wang et
697 al. (2008) also found that the seasonal distributions and variations in rainfall runoff in
698 the permafrost basin were controlled by the freeze-thaw process because of the
699 impermeable nature of the freeze-thaw front and permafrost layer. During the initial
700 ablation period, the supra-permafrost water—whether in the mainstream, the river in
701 the glacier permafrost area, or the river in the permafrost area—was the major
702 recharge source. During the total ablation period, precipitation was the main source of
703 runoff recharge, followed by supra-permafrost water. Although there was little
704 difference the proportion of precipitation and supra-permafrost water during the



705 ablations from 2016 to 2018, precipitation was the major recharge source of runoff in
706 this period. Supra-permafrost water was the main source of runoff recharge in the
707 final ablation period, just as it was in the initial ablation period. In summary, runoff in
708 the cold region during the different ablation periods was mainly composed of runoff
709 from rainfall, meltwater, and supra-permafrost. Because of the inherent seasonal
710 variation in precipitation, there were significant changes in precipitation during the
711 different ablation periods and strong ablation periods in different years. Glacier and
712 snow meltwater was also greatly affected by climatic factors during the different
713 ablation periods, while the supra-permafrost water was relatively stable; the latter
714 became the main source of runoff supply, except for precipitation, in the alpine region.
715 Thus, with the changes that the low temperatures made in the physical properties of
716 the underlying surface, the change in the permafrost had the most significant effect on
717 the hydrological process in cold regions.

718

719 **4.3 Hydrological significance of permafrost**

720

721 The Qinghai-Tibet Plateau (QTP) is the only mid-latitude region in the world that
722 contains permafrost (Zhang et al., 2003). Its permafrost region is located at the source
723 of two major rivers (the Yangtze River and the Yellow River) in China (Yu et al., 2013;
724 2014). Just like the rivers in the Arctic region of Eurasia, they play an important
725 hydrological role in ensuring freshwater recharge and maintaining the ecological
726 security of the basin (Yao et al., 2014; Li et al., 2017; Wang et al., 2019). Permafrost
727 is an objective geological entity developed through the exchange of material and



728 energy between the earth and the atmosphere under the influence of the regional
729 geographic environment, geological structure, lithology, hydrology, and surface
730 characteristics given geologic history and the impact of climate change (Chang et al.,
731 2015). It has its own unique law of evolution and is extremely sensitive to
732 environmental change. The active layer of permafrost is a near-surface soil and rock
733 layer that thaws in the summer and freezes in winter (Wang et al., 2008; 2009; 2017;
734 Chang et al., 2015; Li et al., 2018). Permafrost and active layers are the main factors
735 controlling the hydrometeorological changes of the underlying surface, and the
736 freeze-thaw process of the permafrost active layer is the most important factor
737 affecting the process of runoff. The special water and heat exchange in the active
738 layer of permafrost is the key factor to maintaining the stability of the alpine
739 ecosystem. Permafrost, alpine marsh wetland, and alpine meadow ecosystems have
740 remarkable water conservation functions. They are important factors in stabilizing the
741 water cycle and river runoff in river source areas and have a very important impact on
742 regional ecology and water resource security (Yang et al., 2010; Wu et al., 2015).
743 Under global climate change conditions, permafrost degradation is mainly seen in
744 terms of changes in the active layer. In recent decades, the thickness of permafrost
745 active layers have changed significantly in the Qinghai-Tibet Plateau; since 1980, it
746 has increased by 0.71 cm/a in the eastern part of this region (Zhao et al., 2004). Jin et
747 al. (2006) believe that permafrost in the Qinghai-Tibet Plateau is deteriorating over a
748 large area because of climate change. The observed permafrost data also show a
749 significant increase in the thickness of the active layer in the Qinghai-Tibet Plateau



750 over the past 10 years.

751

752 The permafrost active layer, particularly the hydrothermal environment of the active
753 layer, is the most active and dominant influencing factor at the interface of the
754 ecological environments in cold regions (Yang et al., 2010; Wu et al., 2015; Li et al.,
755 2018). The change in the active layer not only changes the soil water retention
756 capacity, directly affecting the living environment of vegetation, but also changes the
757 soil freeze-thaw process in the active layer. At the same time, the energy-water
758 exchanges accompanied by the freeze-thaw process directly affect the redistribution
759 of soil water and the change in soil water capacity, the movement of water to surface
760 of the frozen soil, and the exchange of latent heat of the water phase transformation.
761 Permafrost reduces the hydraulic conductivity of soil, resulting in the reduction of
762 snow meltwater or precipitation infiltration, changing runoff generation, confluence
763 processes, and characteristics in cold regions (Boucher et al., 2010; Li et al., 2014a;
764 2016b; Mu et al., 2018; Shi et al., 2019).

765

766 Permafrost is the main component of ecosystem in the source area of the Yangtze
767 River. The source of the Yangtze River is in one of the main permafrost districts in the
768 Qinghai-Tibet Plateau. The permafrost area in the study area accounts for 70% of this
769 area (Yao et al., 2014; Li et al., 2017). The change in and distribution of permafrost
770 regions have a significant impact on vegetation and wetlands in this area, as the
771 former is one of the most sensitive to global climate change. The increase in



772 temperature leads to an increase in soil temperature, which deepens the active layer
773 significantly, and causes the permafrost to begin to degenerate. This will certainly
774 lead to significant changes in the ecology and water cycle of the region (McGuire et
775 al., 2002; Walker et al., 2003; Yang et al., 2010).

776

777 In brief, the freeze-thaw of soil in the active layer plays an important role in
778 controlling river runoff. The increase in melting depth leads to a decrease in the direct
779 runoff rate and slow dewatering process. The two processes of runoff retreat are the
780 result of soil freeze-thaw in the active layer. Permafrost has two hydrological
781 functions: on the one hand, permafrost is an impervious layer, and it has the function
782 of preventing surface water or liquid water from infiltrating into deep soil; on the
783 other hand, it forms a soil temperature gradient, which makes the soil moisture close
784 to the ice cover. Therefore, changes in the soil water capacity, soil water permeability,
785 and soil water conductivity, as well as the redistribution of water in the soil profile,
786 are caused by the freeze-thaw of the active layer. The seasonal freeze-thaw process of
787 the active layer directly leads to seasonal flow changes in surface water and
788 groundwater, which affects surface runoff. Climate warming is the main driving force
789 in the degradation of cold ecosystems (Wang et al., 2009; Wu et al., 2015; Li et al.,
790 2018; Wang et al., 2019).

791

792 **5. Conclusions**

793

794 Through systematically analysis of the characteristics of $\delta^{18}\text{O}$, δD , and d-excess of



795 river water in the different ablation periods in 2016 and the total ablation periods from
796 2016 to 2018, the results were as follows.

797 The temporal and spatial characteristics of stable isotopes of river water were
798 significant in the study area. The mean of $\delta^{18}\text{O}$ in TTH was -10.59% , and the mean
799 of d-excess was 9.24% , while the mean of $\delta^{18}\text{O}$ and d-excess in ZMD was -11.99%
800 and 9.66% , respectively. The oxygen isotope in ZMD was more negative than TTH,
801 while the d-excess in ZMD was more positive than TTH. The $\delta^{18}\text{O}$ in mainstream was
802 more negative than that in the glacier permafrost area river and permafrost area river.

803 The influence of evaporation on isotope and d-excess is only prevalent in some places,
804 such as the central and northern parts of the study area in the initial ablation and total
805 ablation periods. However, the influence of evaporation on isotope and d-excess is
806 prevalent in most places except the southeastern part of the study area. Meanwhile,
807 this results also indicated that there may be a hysteresis for the influence of
808 meteorological factors on isotopes and d-excess. The altitude effect is only present
809 during the total ablation periods in 2016 and 2018, and the altitude effect was
810 $-0.16\%/100\text{ m}$ ($p < 0.05$) and $-0.14\%/100\text{ m}$ ($p < 0.05$). The altitude effects were
811 higher for the glacier permafrost area river than those for the mainstream and
812 permafrost in the total ablation period in 2016. Meanwhile, the anti-altitude effect of
813 the glacier permafrost area river was higher than that of the mainstream and
814 permafrost area river. The $\delta^{18}\text{O}$ in the initial and final ablation periods in 2016
815 showed a significant anti-altitude effect for the mainstream and the glacier permafrost
816 area river, while a significant altitude effect appeared in the initial ablation period for



817 the permafrost area river. The slope of LEL for river water showed an increasing trend
818 from initial ablation to final ablation in 2016. Meanwhile, the intercept of LEL for
819 river water also increased from the initial ablation to the final ablation period.

820

821 Moreover, the average of precipitation was 371.9 mm during the sampling period, and
822 the precipitation in the total ablation period accounted for 78.87%. The average of the
823 temperature, relative humidity, and evaporation during the sampling period were
824 -1.42 °C, 52.20%, and 4.14 mm, respectively. However, the average of the
825 temperature, relative humidity, and evaporation in the ablation period were 8.04 °C,
826 66.47%, and 5.57 mm, respectively. Through correlation analysis, it is concluded that:
827 there was a significant negative correlation between the precipitation and $\delta^{18}\text{O}$ at the
828 0.01 level (2-tailed), while a significant positive correlation between precipitation and
829 d-excess. More interestingly, just as with precipitation, significant negative
830 correlations were prevalent between $\delta^{18}\text{O}$ and temperature, relative humidity, and
831 evaporation, with coefficients of -0.671 , -0.555 , and -0.636 , respectively.

832

833 Finally, the mixed segmentation model of the end-member is used to determine the
834 contribution proportion of different water sources to the target water. The results
835 showed that the recharge proportion of precipitation decreased with an increase in
836 altitude in the initial ablation, while the proportions of supra-permafrost water and
837 glacier and snow meltwater showed increasing trends with an increase in altitude.
838 However, the recharge proportion of precipitation was higher than those of the



839 supra-permafrost water and glacier and snow meltwater, and also showed a decreasing
840 trend from low to high altitude in the final ablation period in 2016. The proportion of
841 glacier and snow meltwater increased with an increase in altitude, but the recharge
842 proportion of supra-permafrost water was stable with the change in altitude in the
843 final ablation period in 2016. The proportion of supra-permafrost water was 50.53%
844 in the initial and final ablation periods. Meanwhile, supra-permafrost water was the
845 main recharge source of runoff, followed by precipitation in the total ablation period
846 from 2016 to 2018, and the proportions of precipitation and supra-permafrost water
847 were 36.13% and 36.66%, respectively. The recharge proportion of glacier and snow
848 meltwater was higher in the total ablation period than those in the initial and final
849 ablation periods, with a proportion of 19.44% in the initial and final ablation periods
850 and 27.30% in the total ablation period. Compared with the glacier permafrost area
851 river, the recharge proportion of supra-permafrost water was higher for the permafrost
852 area river than that for the glacier permafrost area river (42.21%). The recharge
853 proportion of supra-permafrost water was 69.54%. Just as with the glacier permafrost
854 area river, the supra-permafrost water was the important recharge source to the runoff
855 in the initial and final ablation periods, and the proportion was 80.97% in the initial
856 and final ablation periods. Meanwhile, the proportion of the supra-permafrost water
857 was 61.92% in the total ablation period. The proportion was higher than that for
858 precipitation (24.13%) in the same period. In general, the supra-permafrost water was
859 the major recharge source for the permafrost area river in the study area. Meanwhile,
860 the glacier and snow meltwater contributed little to the permafrost area river in the



861 initial and final ablation periods. For the mainstream, the proportion was 35.93% in
862 initial and final ablation periods, and 45.55% in the total ablation period. However,
863 the proportion was 47.49% in the initial and final ablation periods, and 36.47% in the
864 total ablation period. The proportion of glacier and snow meltwater for the
865 mainstream (16.59%) was higher than that for the permafrost area river (3.25%) but
866 was lower than that for the glacier permafrost area river (19.44%) in the initial and
867 final ablation periods. Meanwhile, the proportion of glacier and snow meltwater for
868 the mainstream (17.98%) was higher than that for the permafrost area river (13.95%)
869 but was lower than that for the glacier permafrost area river (27.30%) in the total
870 ablation period.

871

872 **Acknowledges**

873

874 This study was supported by National "Plan of Ten Thousand People" Youth Top
875 Talent Project, the Second Tibetan Plateau Scientific Expedition and Research
876 Program(STEP), Grant No. 2019QZKK0405, the Youth Innovation Promotion
877 Association, CAS (2013274), Open funding from the Key Laboratory of Mountain
878 Hazards and Earth Surface Process the open funding from State Key Laboratory of
879 Loess and Quaternary Geology (SKLLQG1814).

880

881 **References**

882

883 Abongwa, P. T., & Atekwana, E. A. : A laboratory study investigating the effects of



- 884 dilution by precipitation on dissolved inorganic carbon and stable isotope
885 evolution in surface waters. Environ Sci Pollu Res, 25(20), 19941-19952.
886 <https://doi.org/10.1007/s11356-018-2085-0>, 2018.
- 887 Banner, J. L., & Hanson, G. N. : Calculation of simultaneous isotopic and trace
888 element variations during water-rock interaction with applications to carbonate
889 diagenesis. Geochim Cosmochim Ac, 54(11), 3123-3137.
890 [https://doi.org/10.1016/0016-7037\(90\)90128-8](https://doi.org/10.1016/0016-7037(90)90128-8), 1990.
- 891 Boucher, J. L., & Carey, S. K.: Exploring runoff processes using chemical, isotopic
892 and hydrometric data in a discontinuous permafrost catchment. Hydro Res, 41(6),
893 508-519. <https://doi.org/10.2166/nh.2010.146>, 2010.
- 894 Chang, J., Wang, G., & Mao, T. : Simulation and prediction of suprapermafrost
895 groundwater level variation in response to climate change using a neural network
896 model. J Hydro, 529, 1211-1220. <https://doi.org/10.1016/j.jhydrol.2015.09.038>,
897 2015.
- 898 Fan, Y., Chen, Y., Li, X., Li, W., & Li, Q. : Characteristics of water isotopes and
899 ice-snowmelt quantification in the Tizinafu River, north Kunlun Mountains,
900 Central Asia. Quater inter, 380, 116-122.
901 <https://doi.org/10.1016/j.quaint.2014.05.020>, 2015.
- 902 Halder, J., Terzer, S., Wassenaar, L. I., Araguás-Araguás, L. J., & Aggarwal, P. K. :
903 The Global Network of Isotopes in Rivers (GNIR): integration of water isotopes
904 in watershed observation and riverine research. Hydrol Earth Sys Sc, 19(8),
905 3419-3431. <https://doi.org/10.5194/hess-19-3419-2015>, 2015.



- 906 Hooper, R. P. : Diagnostic tools for mixing models of stream water chemistry. Water
907 Resour Res, 39(3): 1055. <https://doi.org/10.1029/2002WR001528>, 2003.
- 908 Horita, J., Driesner, T., & Cole, D. R. : Hydrogen isotope fractionation in the system
909 brucite-water±NaCl to elevated temperatures and pressures: Implications for the
910 isotopic property of NaCl fluids under geologic conditions. Geochim
911 Cosmochim Aca, 235, 140-152. <https://doi.org/10.1016/j.gca.2018.05.031>, 2018.
- 912 Gao, H., He, X., Ye, B., & Pu, J. : Modeling the runoff and glacier mass balance in a
913 small watershed on the Central Tibetan Plateau, China, from 1955 to 2008.
914 Hydro Pro, 26(11), 1593-1603. <https://doi.org/10.1002/hyp.8256>, 2012.
- 915 Genereux, D. : Quantifying uncertainty in tracer - based hydrograph separations.
916 Water Resour Res, 34(4), 915-919. <https://doi.org/10.1029/98WR00010>, 1998.
- 917 Gu, W. Z., & Longinelli, A. : A case study on the hydrological significance of stable
918 isotope data on alpine catchments with snow cover and glaciers, Xinjiang, China.
919 IAHS Publications-Publications of the Inter Asso Hydro Sci, 218, 371-384,
920 1993.
- 921 Jin, H., Zhao, L., Wang, S., & Jin, R. : Thermal regimes and degradation modes of
922 permafrost along the Qinghai-Tibet Highway. Sci China Ser D: Earth Sci, 49(11),
923 1170-1183. <https://doi.org/10.1007/s11430-006-2003-z>, 2006.
- 924 Kang, S., Zhang, Y., Qin, D., Ren, J., Zhang, Q., Grigholm, B., & Mayewski, P. A. :
925 Recent temperature increase recorded in an ice core in the source region of
926 Yangtze River. Chinese Sci Bull, 52(6), 825-831.
927 <https://doi.org/10.1007/s11434-007-0140-1>, 2007.



- 928 Klaus, J., & McDonnell, J. J. : Hydrograph separation using stable isotopes: Review
929 and evaluation. J Hydro, 505, 47-64.
930 <https://doi.org/10.1016/j.jhydrol.2013.09.006>, 2013.
- 931 Kong, Y., & Pang, Z. : Evaluating the sensitivity of glacier rivers to climate change
932 based on hydrograph separation of discharge. J Hydro, 434, 121-129.
933 <https://doi.org/10.1016/j.jhydrol.2012.02.029>, 2012.
- 934 Lafrenière, M. J., & Lamoureux, S. F. : Effects of changing permafrost conditions on
935 hydrological processes and fluvial fluxes. Earth-Sci Rev, 191,212-223.
936 <https://doi.org/10.1016/j.earscirev.2019.02.018>, 2019.
- 937 Li, C., Yang, S., Lian, E., Yang, C., Deng, K., & Liu, Z. : Damming effect on the
938 Changjiang (Yangtze River) river water cycle based on stable hydrogen and
939 oxygen isotopic records. J Geochem Explor, 165, 125-133.
940 <https://doi.org/10.1016/j.gexplo.2016.03.006>, 2016.
- 941 Li, Z.X., Qi, F., Wei, L., Tingting, W., Aifang, C., Yan, G., ... & Bing, J. : Study on the
942 contribution of cryosphere to runoff in the cold alpine basin: A case study of
943 Hulugou River Basin in the Qilian Mountains. Global Planet Change, 122,
944 345-361. <https://doi.org/10.1016/j.gloplacha.2014.10.001>, 2014a.
- 945 Li, Z.X., Qi, F., Wei, L., Tingting, W., Yan, G., Yamin, W., ... & Li, L. : Spatial and
946 temporal trend of potential evapotranspiration and related driving forces in
947 Southwestern China, during 1961–2009. Quater inter, 336, 127-144.
948 <https://doi.org/10.1016/j.quaint.2013.12.045>, 2014b.
- 949 Li, Z.X., Qi, F., Wang, Q. J., Song, Y., Aifang, C., & Jianguo, L. : Contribution from



- 950 frozen soil meltwater to runoff in an in-land river basin under water scarcity by
951 isotopic tracing in northwestern China. *Global Planet Change*, 136, 41-51.
952 <https://doi.org/10.1016/j.gloplacha.2015.12.002>, 2016a.
- 953 Li, Z.X., Qi, F., Zongjie, L., Ruifeng, Y., Juan, G., & Yuemin, L. : Climate
954 background, fact and hydrological effect of multiphase water transformation in
955 cold regions of the Western China: A review. *Earth-Sci Re*, 190,33-57.
956 <https://doi.org/10.1016/j.earscirev.2018.12.004>, 2018.
- 957 Li, Z.X., Qi, F., Wang, Q. J., Song, Y., Jianguo, L., Yongge, L., & Yamin, W. :
958 Quantitative evaluation on the influence from cryosphere meltwater on runoff in
959 an inland river basin of China. *Global Planet Change*, 143, 189-195.
960 <https://doi.org/10.1016/j.gloplacha.2016.06.005>, 2016b.
- 961 Li, Z.X., Qi, F., Wei, L., Tingting, W., Xiaoyan, G., Zongjie, L., ... & Yaoxuan, S. :
962 The stable isotope evolution in Shiyi glacier system during the ablation period in
963 the north of Tibetan Plateau, China. *Quater inter*, 380, 262-271.
964 <https://doi.org/10.1016/j.quaint.2015.02.013>, 2015.
- 965 Li, Z., Yuan, R., Feng, Q., Zhang, B., Lv, Y., Li, Y., ... & Shi, Y. : Climate background,
966 relative rate, and runoff effect of multiphase water transformation in Qilian
967 Mountains, the third pole region. *Sci Total Environ*, 663, 315-328.
968 <https://doi.org/10.1016/j.scitotenv.2019.01.339>, 2019.
- 969 Li, Z.J., Song, L. L., Jing-zhu, M., & Li, Y. G. : The characteristics changes of pH and
970 EC of atmospheric precipitation and analysis on the source of acid rain in the
971 source area of the Yangtze River from 2010 to 2015. *Atmos environ*, 156, 61-69.



- 972 <https://doi.org/10.1016/j.atmosenv.2017.02.025>, 2017.
- 973 Li, Z.J., Zong-Xing, L., Ling-Ling, S., Jin-Zhu, M., & Yong, S. : Environment
974 significance and hydrochemical characteristics of supra-permafrost water in the
975 source region of the Yangtze River. *Sci total environ*, 644, 1141-1151.
976 <https://doi.org/10.1016/j.scitotenv.2018.07.029>, 2018.
- 977 Liang, E., Shao, X., & Qin, N. : Tree-ring based summer temperature reconstruction
978 for the source region of the Yangtze River on the Tibetan Plateau. *Global Planet*
979 *Change*, 61(3-4), 313-320. <https://doi.org/10.1016/j.gloplacha.2007.10.008>,
980 2008.
- 981 Liu, F., Williams, M. W., & Caine, N. : Source waters and flow paths in an alpine
982 catchment, Colorado Front Range, United States. *Water Resour Res*, 40(9), 1-17.
983 <https://doi.org/10.1029/2004WR003076>, 2004.
- 984 Lutz, A. F., Immerzeel, W. W., Shrestha, A. B., & Bierkens, M. F. P. : Consistent
985 increase in High Asia's runoff due to increasing glacier melt and precipitation.
986 *Nat Clim Change*, 4(7), 587. <https://doi.org/10.1038/nclimate2237>, 2014.
- 987 Maurya, A. S., Shah, M., Deshpande, R. D., Bhardwaj, R. M., Prasad, A., & Gupta, S.
988 K. : Hydrograph separation and precipitation source identification using stable
989 water isotopes and conductivity: River Ganga at Himalayan foothills. *Hydro Pro*,
990 25(10), 1521-1530. <https://doi.org/10.1002/hyp.7912>, 2011.
- 991 McGuire, A. D., Wirth, C., Apps, M., Beringer, J., Klein, J., Epstein, H., ... & Efremov,
992 D. : Environmental variation, vegetation distribution, carbon dynamics and
993 water/energy exchange at high latitudes. *J Veget Sci*, 13(3), 301-314.



- 994 <https://doi.org/10.1111/j.1654-1103.2002.tb02055.x>, 2002.
- 995 Mu, Y., Ma, W., Li, G., Niu, F., Liu, Y., & Mao, Y. : Impacts of supra-permafrost
996 water ponding and drainage on a railway embankment in continuous permafrost
997 zone, the interior of the Qinghai-Tibet Plateau. *Cold Reg Sci Tech*, 154, 23-31.
998 <https://doi.org/10.1016/j.coldregions.2018.06.007>, 2018.
- 999 Orłowski, N., Breuer, L., & McDonnell, J. J. : Critical issues with cryogenic
1000 extraction of soil water for stable isotope analysis. *Ecohydro*, 9(1), 1-5.
1001 <https://doi.org/10.1002/eco.1722>, 2016.
- 1002 Pan, X., Yu, Q., You, Y., Chun, K. P., Shi, X., & Li, Y. : Contribution of
1003 supra-permafrost discharge to thermokarst lake water balances on the
1004 northeastern Qinghai-Tibet Plateau. *J Hydro*, 555, 621-630.
1005 <https://doi.org/10.1016/j.jhydrol.2017.10.046>, 2017.
- 1006 Peng, T. R., Wang, C. H., Huang, C. C., Fei, L. Y., Chen, C. T. A., & Hwong, J. L. :
1007 Stable isotopic characteristic of Taiwan's precipitation: A case study of western
1008 Pacific monsoon region. *Earth Planet Sci Let*, 289(3-4), 357-366.
1009 <https://doi.org/10.1016/j.epsl.2009.11.024>, 2010.
- 1010 Prasher, M., Mauser, W., & Weber, M. : Quantifying present and future glacier
1011 melt-water contribution to runoff in a central Himalayan river basin. *Cryos*, 7(3).
1012 <https://doi:10.5194/tc-7-889-2013>, 2013.
- 1013 Pu, T., He, Y., Zhu, G., Zhang, N., Du, J., & Wang, C. : Characteristics of water stable
1014 isotopes and hydrograph separation in Baishui catchment during the wet season
1015 in Mt. Yulong region, south western China. *Hydro Pro*, 27(25), 3641-3648.



- 1016 <https://doi.org/10.1002/hyp.9479>, 2013.
- 1017 Pu, J. : Glacier Inventory of China: The Yangtze River Drainage Basin. Lanzhou:
1018 Gansu Culture Press, 1-81, 1994.
- 1019 Qu, J. H., Lu, S. B., Gao, Z. P., Li, W., Li, Z., & Yu, F. : Research on
1020 hydrogeochemical characteristics and transformation relationships between surface
1021 water and groundwater in the Weihe River. Hydrol Earth sys sc,1-14.
1022 <https://doi.org/10.5194/hess-2017-654>, 2017.
- 1023 Shi, Y., Niu, F., Lin, Z., & Luo, J. : Freezing/thawing index variations over the
1024 circum-Arctic from 1901 to 2015 and the permafrost extent. Sci Total Environ,
1025 660, 1294-1305. <https://doi.org/10.1016/j.scitotenv.2019.01.121>, 2019.
- 1026 Uhlenbrook, S., & Hoeg, S. : Quantifying uncertainties in tracer - based hydrograph
1027 separations: a case study for two - , three - and five - component hydrograph
1028 separations in a mountainous catchment. Hydro Pro, 17(2), 431-453.
1029 <https://doi.org/10.1002/hyp.1134>, 2003.
- 1030 Walker, D. A., Jia, G. J., Epstein, H. E., Reynolds, M. K., Chapin Iii, F. S., Copass,
1031 C., ... & Nelson, F. : Vegetation - soil - thaw - depth relationships along a
1032 low - arctic bioclimate gradient, Alaska: Synthesis of information from the
1033 ATLAS studies. Perma Peri Pro, 14(2), 103-123. <https://doi.org/10.1002/ppp.452>,
1034 2003.
- 1035 Wang, G., Liu, G., & Liu, L. A. : Spatial scale effect on seasonal streamflows in
1036 permafrost catchments on the Qinghai–Tibet Plateau. Hydro Pro, 26(7), 973-984.
1037 <https://doi.org/10.1002/hyp.8187>, 2012.
- 1038 Wang, G., Hu, H., & Li, T. : The influence of freeze–thaw cycles of active soil layer



- 1039 on surface runoff in a permafrost watershed. *J Hydro*, 375(3-4), 438-449.
1040 <https://doi.org/10.1016/j.jhydrol.2009.06.046>, 2009.
- 1041 Wang, G., Tianxu, M., Juan, C., Chunlin, S., & Kewei, H. : Processes of runoff
1042 generation operating during the spring and autumn seasons in a permafrost
1043 catchment on semi-arid plateaus. *J hydro*, 550, 307-317.
1044 <https://doi.org/10.1016/j.jhydrol.2017.05.020>, 2017.
- 1045 Wang, G., Yuanshou, L., Yibo, W., & Qingbo, W. : Effects of permafrost thawing on
1046 vegetation and soil carbon pool losses on the Qinghai–Tibet Plateau, China.
1047 *Geoderma*, 143(1-2), 143-152. <https://doi.org/10.1016/j.geoderma.2007.10.023>,
1048 2008.
- 1049 Wang, T., Wu, T., Wang, P., Li, R., Xie, C., & Zou, D. : Spatial distribution and
1050 changes of permafrost on the Qinghai-Tibet Plateau revealed by statistical
1051 models during the period of 1980 to 2010. *Sci Total Environ*, 650, 661-670.
1052 <https://doi.org/10.1016/j.scitotenv.2018.08.398>, 2019.
- 1053 Wang, X., Chen, R., Liu, G., Yang, Y., Song, Y., Liu, J., ... & Wang, L. : Spatial
1054 distributions and temporal variations of the near-surface soil freeze state across
1055 China under climate change. *Global planet change*, 172, 150-158.
1056 <https://doi.org/10.1016/j.gloplacha.2018.09.016>, 2019.
- 1057 West, A. G., February, E. C., & Bowen, G. J. : Spatial analysis of hydrogen and
1058 oxygen stable isotopes (“isoscapes”) in ground water and tap water across South
1059 Africa. *J Geochem Explo*, 145, 213-222.
1060 <https://doi.org/10.1016/j.gexplo.2014.06.009>, 2014.



- 1061 Wu, Q., Hou, Y., Yun, H., & Liu, Y. : Changes in active-layer thickness and
1062 near-surface permafrost between 2002 and 2012 in alpine ecosystems,
1063 Qinghai–Xizang (Tibet) Plateau, China. *Global Planet Change*, 124, 149-155.
1064 <https://doi.org/10.1016/j.gloplacha.2014.09.002>, 2015.
- 1065 Yang, L., Song, X., Zhang, Y., Han, D., Zhang, B., & Long, D. : Characterizing
1066 interactions between surface water and groundwater in the Jialu River basin
1067 using major ion chemistry and stable isotopes. *Hydrol Earth Sys Sc*, 16(11),
1068 4265-4277. <https://doi.org/10.5194/hess-16-4265-2012>, 2012.
- 1069 Yang, M., Nelson, F. E., Shiklomanov, N. I., Guo, D., & Wan, G. : Permafrost
1070 degradation and its environmental effects on the Tibetan Plateau: A review of
1071 recent research. *Earth-Sci Re*, 103(1-2), 31-44.
1072 <https://doi.org/10.1016/j.earscirev.2010.07.002>, 2010.
- 1073 Yang, Q., Mu, H., Wang, H., Ye, X., Ma, H., & Martín, J. D. : Quantitative evaluation
1074 of groundwater recharge and evaporation intensity with stable oxygen and
1075 hydrogen isotopes in a semi - arid region, Northwest China. *Hydro pro*, 32(9),
1076 1130-1136. <https://doi.org/10.1002/hyp.11474>, 2018.
- 1077 Yao, Z., Liu, Z., Huang, H., Liu, G., & Wu, S. : Statistical estimation of the impacts of
1078 glaciers and climate change on river runoff in the headwaters of the Yangtze
1079 River. *Quater inter*, 336, 89-97. <https://doi.org/10.1016/j.quaint.2013.04.026>,
1080 2014.
- 1081 Yu, G. A., Liu, L., Li, Z., Li, Y., Huang, H., Brierley, G., ... & Pan, B. : Fluvial
1082 diversity in relation to valley setting in the source region of the Yangtze and



- 1083 Yellow Rivers. J Geog Sci, 23(5), 817-832.
1084 <https://doi.org/10.1007/s11442-013-1046-2>, 2013.
- 1085 Yu, G. A., Brierley, G., Huang, H. Q., Wang, Z., Blue, B., & Ma, Y. : An
1086 environmental gradient of vegetative controls upon channel planform in the
1087 source region of the Yangtze and Yellow Rivers. Catena, 119, 143-153.
1088 <https://doi.org/10.1016/j.catena.2014.02.010>, 2014.
- 1089 Zhang, Y., Ohata, T., & Kadota, T. : Land-surface hydrological processes in the
1090 permafrost region of the eastern Tibetan Plateau. J Hydro, 283(1-4), 41-56.
1091 [https://doi.org/10.1016/S0022-1694\(03\)00240-3](https://doi.org/10.1016/S0022-1694(03)00240-3), 2003.
- 1092 Zhao, L., Ping, C. L., Yang, D., Cheng, G., Ding, Y., & Liu, S. : Changes of climate
1093 and seasonally frozen ground over the past 30 years in Qinghai–Xizang (Tibetan)
1094 Plateau, China. Global Planet Change, 43(1-2), 19-31.
1095 <https://doi.org/10.1016/j.gloplacha.2004.02.003>, 2004.
- 1096 Zhu, X., Wu, T., Zhao, L., Yang, C., Zhang, H., Xie, C., ... & Du, Y. : Exploring the
1097 contribution of precipitation to water within the active layer during the thawing
1098 period in the permafrost regions of central Qinghai-Tibet Plateau by stable
1099 isotopic tracing. Sci Total Environ, 661, 630-644.
1100 <https://doi.org/10.1016/j.scitotenv.2019.01.064>, 2019.
- 1101
1102
1103
1104



1105 **Tables:**

1106

1107 Table 1 The correlation analysis of $\delta^{18}\text{O}$ and d-excess and meteorological factors in
1108 the fixed point (TTH and ZMD) from March,16 to July, 18.

1109

1110

1111

1112

1113

1114

1115

1116

1117

1118

1119

1120

1121

1122

1123

1124

1125

1126

1127

1128

1129

1130

1131

1132

1133

1134



1135 Table 1 The correlation analysis of $\delta^{18}\text{O}$ and d-excess and meteorological factors in
 1136 the fixed point (TTH and ZMD) from March,16 to July, 18.

	Precipitation (mm)	Temperature (°C)	Ralative humidity (%)	Evaporation (mm)	$\delta^{18}\text{O}(\text{‰})$	D-excess (‰)
Precipitation(mm)	1					
Temperature(°C)	0.853**	1				
Ralative humidity(%)	0.760**	0.836**	1			
Evaporation(mm)	0.658**	0.865**	0.586**	1		
$\delta^{18}\text{O}(\text{‰})$	-0.518**	-0.671**	-0.555**	-0.636**	1	
D-excess(‰)	0.500**	0.602**	0.524**	0.533**	-0.568**	1

1137 Note: **, Correlation is significant at the 0.01 level (2-tailed).

1138
 1139
 1140
 1141
 1142
 1143
 1144
 1145
 1146
 1147
 1148
 1149
 1150
 1151
 1152
 1153
 1154
 1155
 1156
 1157
 1158
 1159
 1160
 1161
 1162
 1163
 1164
 1165
 1166
 1167
 1168



1169 **Figures:**

1170 Fig.1 The map of the study area and the sampling point of river water in different
1171 ablation period

1172 (Fig.1a was the detail location of the study area in China and Asian and the distribution of fixed
1173 point for precipitation, river water and glacier and snow meltwater; Fig.1b was the distribution of
1174 sampling point in initial ablation in 2016; Fig.1c was the distribution of sampling point in ablation
1175 in 2016; Fig.1d was the distribution of sampling point in end ablation in 2016; Fig.1e was the
1176 distribution of sampling point in ablation in 2017; Fig.1f was the distribution of sampling point in
1177 ablation in 2018)

1178 Fig.2 Variation of meteorological factors during sampling period

1179 (Shadow represents the ablation period)

1180 Fig.3 Temporal variation of $\delta^{18}\text{O}$ and d-excess during the sampling period in study
1181 area

1182 (This figure mainly showed the temporal variation of $\delta^{18}\text{O}$ and d-excess for different type runoff
1183 based on different ablation in 2016 and strong ablation from 2016 to 2018; Fig.2a, b, c showed the
1184 change of $\delta^{18}\text{O}$ and d-excess in different ablation period for mainstream, glacier and snow runoff
1185 and river in permafrost area; Fig.2d, e, f showed the change of $\delta^{18}\text{O}$ and d-excess in ablation
1186 period from 2016 to 2018 for mainstream, glacier and snow runoff and river in permafrost area)

1187 Fig.4 Spatial variation of $\delta^{18}\text{O}$ based on different ablation in 2016 and ablation from
1188 2016 to 2018

1189 Fig.5 Spatial variation of d-excess based on different ablation in 2016 and ablation
1190 from 2016 to 2018



1191 Fig.6 The variation of $\delta^{18}\text{O}$ and d-excess with the altitude change in study area
1192 (Fig.6a was the variation of $\delta^{18}\text{O}$ and d-excess with the altitude change for mainstream; Fig.6b
1193 was the variation of $\delta^{18}\text{O}$ and d-excess with the altitude change for river in glacier permafrost
1194 area;Fig.6c was the variation of $\delta^{18}\text{O}$ and d-excess with the altitude change for river in permafrost
1195 area; IA in 2016 represents Initial ablation in 2016; A in 2016 represents Ablation in 2016; EA in
1196 2016 represents End ablation in 2016; A in 2017 represents Ablation in 2017; A in 2018
1197 represents Ablation in 2018)
1198 Fig.7 The distribution of δD and $\delta^{18}\text{O}$ for river water among other water bodies in
1199 study area
1200 (Fig.7a was the plot of $\delta^{18}\text{O}$ for river water in different type, supra-permafrost water, glacier snow
1201 meltwater and precipitation; Fig.7b was the plot of δD for river water in different type,
1202 supra-permafrost water, glacier snow meltwater and precipitation; Fig.7c was the plot of δD
1203 versus $\delta^{18}\text{O}$ for river water, supra-permafrost water, glacier snow meltwater and precipitation)
1204 Fig.8 Three end element diagram using the mean values of $\delta^{18}\text{O}$ and d-excess for river
1205 water in different ablation in 2016 and ablation from 2016 to 2018
1206 Fig.9 Recharge proportion from possible sources to river water in different altitude
1207 during different ablation in 2016 and ablation from 2016 to 2018
1208 Fig.10 The variation of location evaporation line (LEL) of river water based on
1209 different ablation in 2016 and ablation from 2016 to 2018
1210 Fig.11 Conceptual model map of the recharge form and proportion of the river water
1211 in different ablation period
1212 (Dark green represents the basin of river in permafrost area; Gray and light green represents the



1213 basin of the river in glacier permafrost area)

1214

1215

1216

1217

1218

1219

1220

1221

1222

1223

1224

1225

1226

1227

1228

1229

1230

1231

1232

1233

1234

1235

1236

1237

1238

1239

1240

1241

1242

1243

1244

1245

1246

1247

1248

1249

1250

1251

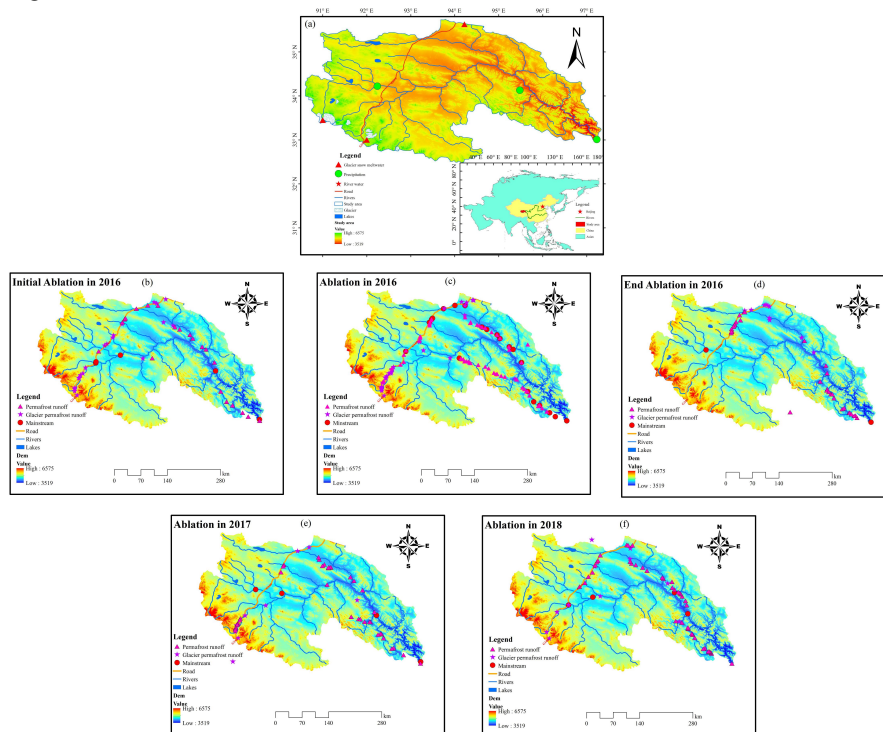
1252

1253

1254



1255 Fig.1



1256

1257 Fig.1 The map of the study area and the sampling point of river water in different
1258 ablation period (Fig.1a was the detail location of the study area in China and Asian and the
1259 distribution of fixed point for precipitation, river water and glacier and snow meltwater; Fig.1b
1260 was the distribution of sampling point in initial ablation in 2016; Fig.1c was the distribution of
1261 sampling point in ablation in 2016; Fig.1d was the distribution of sampling point in end ablation in
1262 2016; Fig.1e was the distribution of sampling point in ablation in 2017; Fig.1f was the distribution
1263 of sampling point in ablation in 2018)

1264

1265

1266

1267

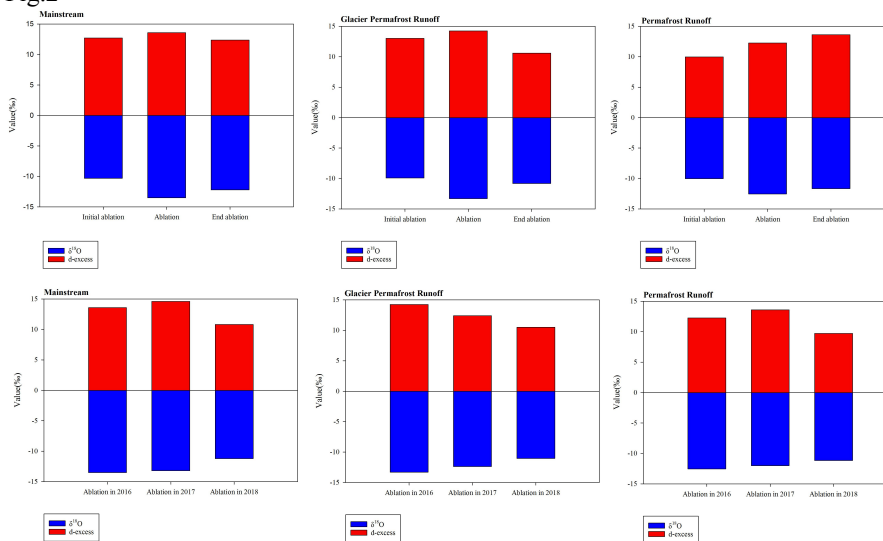
1268

1269

1270



1271 Fig.2



1272

1273 Fig.2 Variation of meteorological factors during sampling period (Shadow represents the

1274 ablation period)

1275

1276

1277

1278

1279

1280

1281

1282

1283

1284

1285

1286

1287

1288

1289

1290

1291

1292

1293

1294

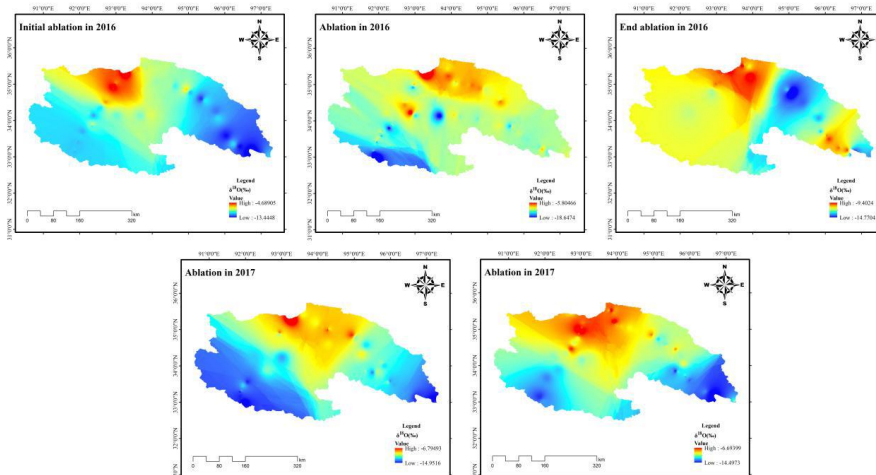
1295

1296

1297



1298 Fig.3



1299

1300 Fig.3 Temporal variation of $\delta^{18}\text{O}$ and d-excess during the sampling period in study
1301 area (This figure mainly showed the temporal variation of $\delta^{18}\text{O}$ and d-excess for different type
1302 runoff based on different ablation in 2016 and strong ablation from 2016 to 2018; Fig.2a, b, c
1303 showed the change of $\delta^{18}\text{O}$ and d-excess in different ablation period for mainstream, glacier and
1304 snow runoff and river in permafrost area; Fig.2d, e, f showed the change of $\delta^{18}\text{O}$ and d-excess in
1305 ablation period from 2016 to 2018 for mainstream, glacier and snow runoff and river in permafrost

1306 area)

1307

1308

1309

1310

1311

1312

1313

1314

1315

1316

1317

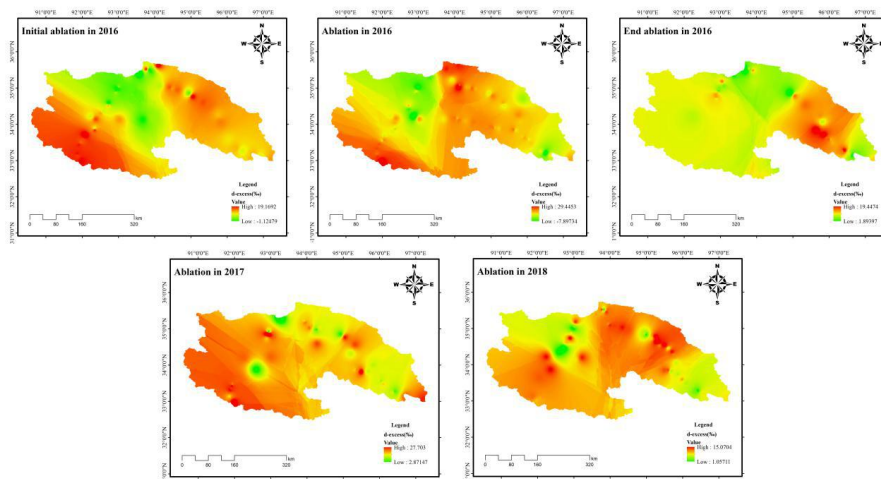
1318

1319

1320



1321 Fig.4



1322

1323 Fig.4 Spatial variation of $\delta^{18}\text{O}$ based on different ablation in 2016 and ablation from

1324 2016 to 2018

1325

1326

1327

1328

1329

1330

1331

1332

1333

1334

1335

1336

1337

1338

1339

1340

1341

1342

1343

1344

1345

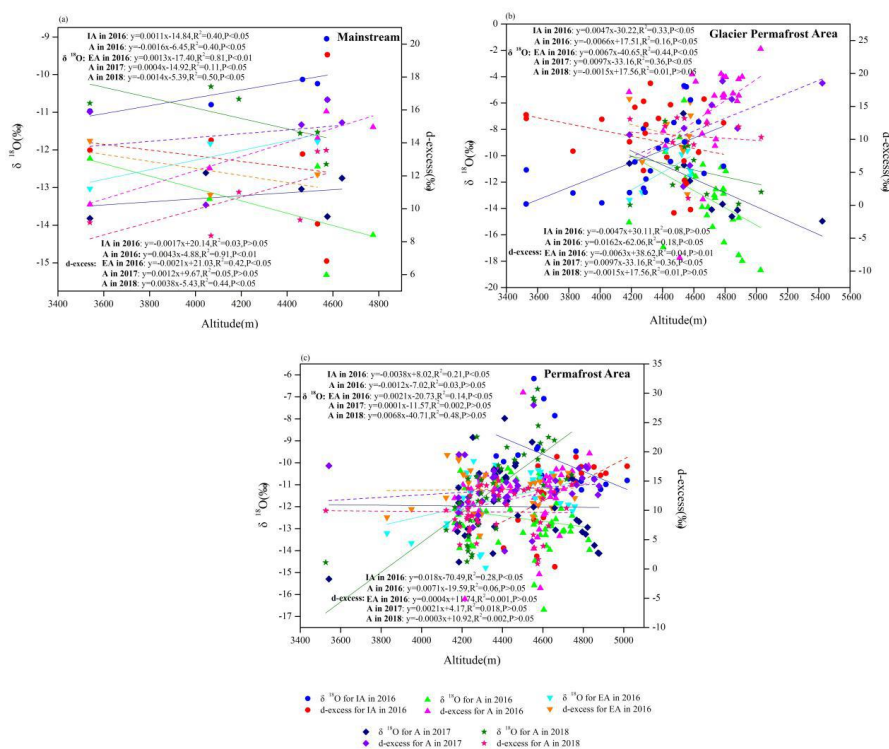
1346

1347

1348



1349 Fig.5



1350

1351 Fig.5 Spatial variation of d-excess based on different ablation in 2016 and ablation

1352 from 2016 to 2018

1353

1354

1355

1356

1357

1358

1359

1360

1361

1362

1363

1364

1365

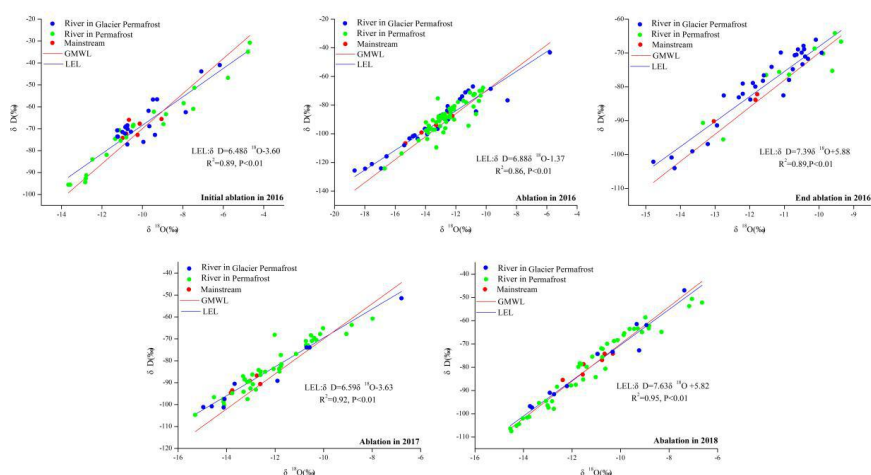
1366

1367

1368



1369 Fig.6



1370

1371 Fig.6 The variation of $\delta^{18}\text{O}$ and d-excess with the altitude change in study area

1372 (Fig.6a was the variation of $\delta^{18}\text{O}$ and d-excess with the altitude change for mainstream; Fig.6b

1373 was the variation of $\delta^{18}\text{O}$ and d-excess with the altitude change for river in glacier permafrost

1374 area; Fig.6c was the variation of $\delta^{18}\text{O}$ and d-excess with the altitude change for river in permafrost

1375 area; IA in 2016 represents Initial ablation in 2016; A in 2016 represents Ablation in 2016; EA in

1376 2016 represents End ablation in 2016; A in 2017 represents Ablation in 2017; A in 2018

1377 represents Ablation in 2018)

1378

1379

1380

1381

1382

1383

1384

1385

1386

1387

1388

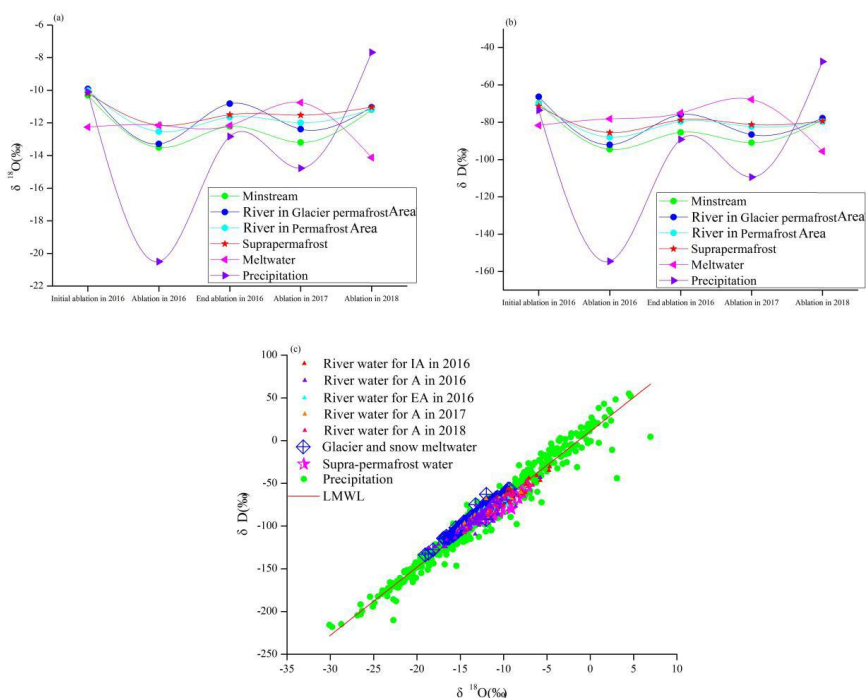
1389

1390

1391



1392 Fig.7



1393

1394

1395 Fig.7 The distribution of δD and $\delta^{18}\text{O}$ for river water among other water bodies in
1396 study area (Fig.7a was the plot of $\delta^{18}\text{O}$ for river water in different type, supra-permafrost water,
1397 glacier snow meltwater and precipitation; Fig.7b was the plot of δD for river water in different
1398 type, supra-permafrost water, glacier snow meltwater and precipitation; Fig.7c was the plot of δD
1399 versus $\delta^{18}\text{O}$ for river water, supra-permafrost water, glacier snow meltwater and precipitation)

1400

1401

1402

1403

1404

1405

1406

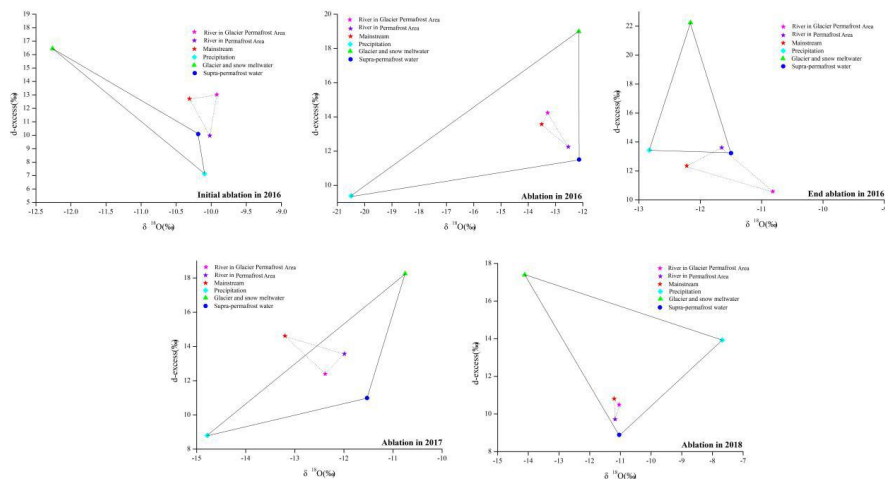
1407

1408

1409



1410 Fig.8



1411

1412 Fig.8 Three end element diagram using the mean values of $\delta^{18}\text{O}$ and d-excess for river

1413 water in different ablation in 2016 and ablation from 2016 to 2018

1414

1415

1416

1417

1418

1419

1420

1421

1422

1423

1424

1425

1426

1427

1428

1429

1430

1431

1432

1433

1434

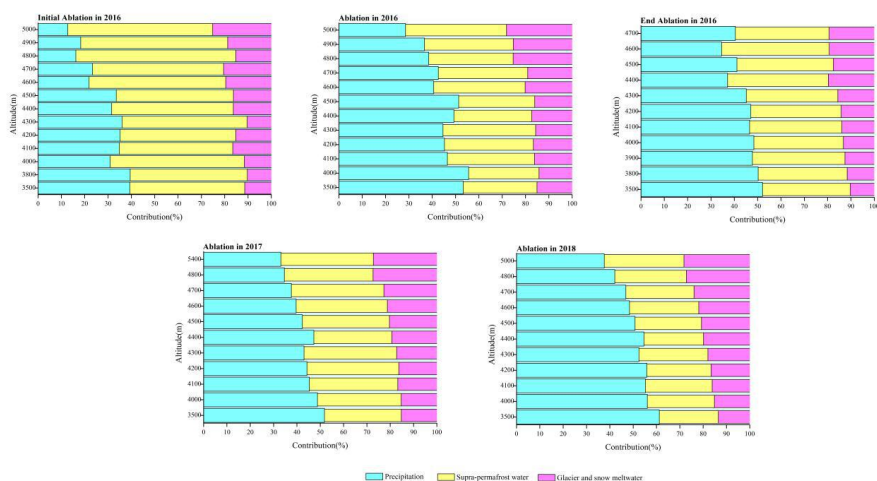
1435

1436

1437



1438 Fig.9



1439

1440 Fig.9 Recharge proportion from possible sources to river water in different altitude

1441 during different ablation in 2016 and ablation from 2016 to 2018

1442

1443

1444

1445

1446

1447

1448

1449

1450

1451

1452

1453

1454

1455

1456

1457

1458

1459

1460

1461

1462

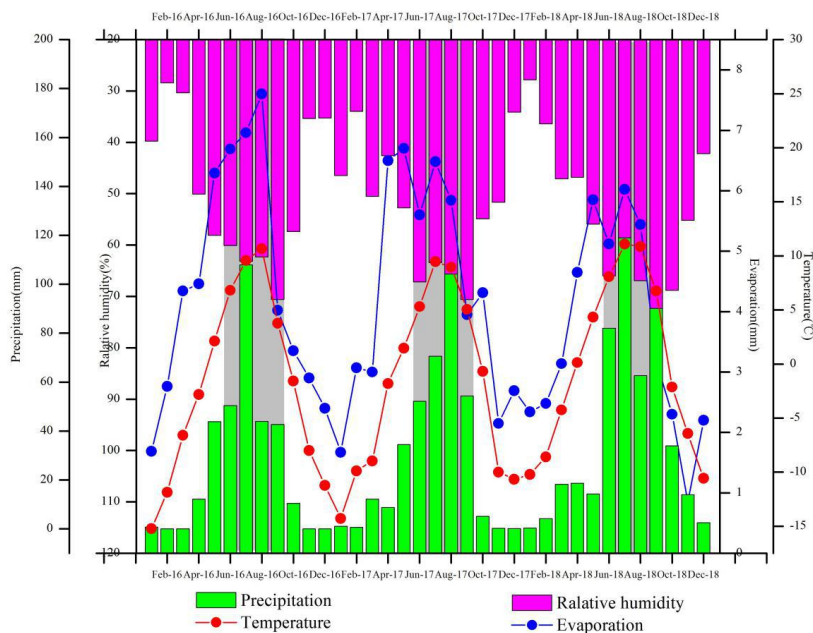
1463

1464

1465



1466 Fig.10



1467

1468 Fig.10 The variation of location evaporation line (LEL) of river water based on

1469 different ablation in 2016 and ablation from 2016 to 2018

1470

1471

1472

1473

1474

1475

1476

1477

1478

1479

1480

1481

1482

1483

1484

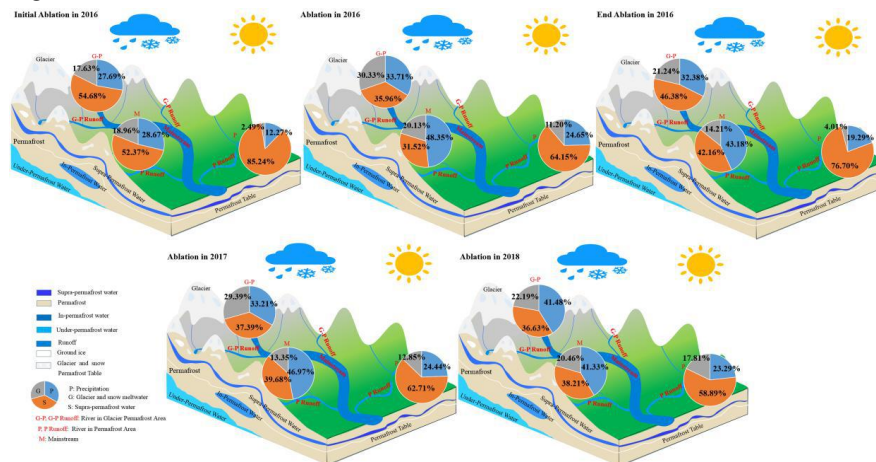
1485

1486

1487



1488 Fig.11



1489

1490 Fig.11 Conceptual model map of the recharge form and proportion of the river water

1491 in different ablation period (Dark green represents the basin of river in permafrost area; Gray

1492 and light green represents the basin of the river in glacier permafrost area)